DOE/MC/26034--3083

DE92 001269

Catalytic Carbon Membranes for Hydrogen Production

Final Report

A.S. Damle
S.K. Gangwal

Work Performed Under Contract No.: DE-AC21-89MC26034

For
U.S. Department of Energy
Office of Fossil Energy
Morgantown Energy Technology Center
P.O. Box 880
Morgantown, West Virginia 26507-0880

By
Research Triangle Institute
P.O. Box 12194
Research Triangle Park, North Carolina 27709-2194

January 1992

ABSTRACT

Commercial carbon composite microfiltration membranes may be modified for gas separation applications by providing a gas separation layer with pores in the 1- to 10-nm range. Several organic polymeric precursors and techniques for depositing a suitable layer were investigated in this project. The in situ polymerization technique was found to be the most promising, and pure component permeation tests with membrane samples prepared with this technique indicated Knudsen diffusion behavior. The gas separation factors obtained by mixed-gas permeation tests were found to depend strongly on gas temperature and pressure indicating significant viscous flow at high-pressure conditions. The modified membranes were used to carry out simultaneous water gas shift reaction and product hydrogen separation. These tests indicated increasing CO conversions with increasing hydrogen separation. A simple process model was developed to simulate a catalytic membrane reactor. A number of simulations were carried out to identify operating conditions leading to product hydrogen concentrations over 90 percent.

ACKNOWLEDGMENTS

This research was sponsored by the Morgantown Energy Technology Center (METC) of the U.S. Department of Energy (DOE) under Contract No. DE-AC21-89MC26034.

Valuable technical guidance and frequent discussion by the U.S. DOE/METC technical project managers Dr. V.K. Venkataraman and Dr. J. Longanbach are gratefully acknowledged.

Cooperation by Carbone U.S.A. Corporation in supplying the carbon composite tubular microfiltration membranes is gratefully acknowledged. Dr. Hubert Fleming of GFT Corporation (now with Zeron Environmental, Inc.) provided valuable technical input during initial stages of this project.

Technical and clerical assistance from Gary Howe, Ernest Johnson, Teresa Paar, Chris Fuller, Jan Shirley, and Sue Pauley is sincerely acknowledged.

TABLE OF CONTENTS

LIST OF TABLES

LIST OF FIGURES

LIST OF FIGURES (continued)

Number **Page**

EXECUTIVE SUMMARY

In direct coal liquefaction processes, the production, efficient use, and recovery of hydrogen account for over 50 percent of the capital cost. Conventional hydrogen plants for coal liquefaction typically employ coal gasification followed by water-gas shift (WGS) reaction, complicated liquid phase processing steps for hydrogen sulfide removal, Claus/Scot sulfur recovery, and hydrogen separation, e.g., by pressure swing adsorption. One possible approach to reduce the cost of hydrogen production is to combine the WGS reaction and hydrogen separation steps in one catalytic membrane reactor unit. To utilize such an approach, a hydrogen-selective catalytic membrane reactor is needed, capable of operating at up to 20 atm and 300 to 500 °C with hydrogen sulfide containing gasifier gas streams. The objective of this project is to evaluate the feasibility of the development of carbon composite membrane reactors for carrying out simultaneous WGS reaction and hydrogen separation.

Commercially available carbon composite microfiltration membranes have pore sizes in the range of 0.1 to 1.0 μm that must be reduced considerably to make them suitable for gas separation applications. The approach used in this project to modify the commercial carbon membranes is to deposit a layer of an organic polymeric precursor on the existing microfiltration layer followed by controlled pyrolysis to convert the organic layer into carbon. Four techniques were investigated for depositing a layer of a suitable organic precursor: dip coating of a polymer precursor solution, gas phase plasma polymerization of a monomer, in situ polymerization of a monomer, and gas phase-pyrolysis of organic vapors to deposit carbon. Polymer precursor materials investigated in this project include polyacrylonitrile (PAN), polyfurfuryl alcohol (PFA), phenol-formaldehyde resin, cellulose, furfuryl alcohol-phenolic (FAP) resin, and propylene. The effect of coating parameters and subsequent pyrolysis conditions on the permeation characteristics of the resulting membrane was investigated for different precursors and coating techniques. The performance of the modified membranes was determined by measuring permeation rates of pure gases as well as by conducting mixed-gas permeation tests to determine the gas separation factors.

Precursor deposition techniques based on polymer solution coating, plasma polymerization, and gas-phase pyrolysis decreased the gas permeation rates significantly. However, these techniques apparently did not provide adequate reduction in the membrane pore size to yield a significant gas separation based on Knudsen diffusion mechanism. The in situ polymerization technique was found to be much more promising than other techniques. Pure (single) gas permeation tests with membrane samples prepared using this technique indicated permeation rates to be inversely proportional to the square root of the molecular weight, thus indicating a predominantly diffusive flow. The hydrogen permeabilities of these membranes ranged from $1x10^{-5}$ to $5x10^{-5}$ std $cm^3/(s \cdot cm^2 \cdot mm\ Hg)$ as compared to $6x10^{-3}$ std $cm^3/(s \cdot cm^2 \cdot mm\ Hg)$ for an unmodified carbon microfiltration tube. The gas separation factors obtained with these samples in mixed-gas (multiple gases) permeation tests were found to depend strongly on gas temperature and pressure. The observed separation factors for the membranes modified by the in situ polymerization technique were significantly higher than those for

unmodified membranes, indicating significant reduction in membrane pore size. However, these separation factors were lower than the theoretical maximum values expected for Knudsen diffusion separation, indicating significant viscous flow along with diffusion at high-pressure conditions.

Although the observed separation factors were less than the theoretical maximum values, the ability of these membranes to increase CO conversion in WGS reaction by simultaneous separation of hydrogen was experimentally verified. Experiments were conducted with typical Manufacturing and Technology Conversion International, Inc. (MTCI) gasifier gas composition using 2:1 to 4:1 mol ratios of steam to CO. In these experiments the amount of hydrogen permeated was controlled by the transmembrane pressure drop. Increasing the transmembrane pressure drop was generally found to increase CO conversion moderately. Due to low permeation rates and a limited membrane surface area that could be used in these experimental studies, only a small fraction of the feed gas was permeated across the membrane with the stage cuts on the order of 0.1 or less.

Computer simulations were conducted to determine the potential of increased CO conversion due to hydrogen separation with gas separation factors based on Knudsen diffusion. The simulations indicated that high feed pressure to permeate pressure ratios are necessary to increase CO conversion and product hydrogen concentration significantly. With an H_2O:CO mol ratio of 2:1, the CO conversion was predicted to increase from 58 to 75 percent with a pressure ratio of 20 and a stage cut of 0.65. The corresponding product hydrogen concentration increased from 54 to 71 percent (dry basis). To increase the product hydrogen concentration further a multistage process is necessary. For a two-stage process with a pressure ratio of 20 in each stage and stage cuts of 0.75 and 0.65, respectively, the hydrogen concentration in the product stream could be increased to 82.5 percent with an overall CO conversion of 86.2 and 78.7 percent recovery of hydrogen.

Simulations were conducted with both cocurrent and countercurrent permeate flows with respect to feed flow direction. For the cases studied, countercurrent flow simulations predicted slightly greater CO conversions and product hydrogen concentrations than those for cocurrent flow schemes. The difference was minimal for high-pressure ratios and increased with decreasing pressure ratio.

The simulated membrane performance, of course, depends strongly on the gas separation factors used. Simulations conducted with the observed gas separation factors, which were lower than the theoretical maximum for Knudsen diffusion, indicated a much smaller increase in CO conversion and product hydrogen concentration. For example, simulations conducted with a H_2/CO_2 separation factor of 2 (as observed in high-pressure permeation tests) with a H_2O:CO mol ratio of 3:1 and MTCI gasifier gas composition indicated an increase in CO conversion from 70.6 to 72.1 percent for a pressure ratio of 20 and stage cut of 0.65. The corresponding increase in product hydrogen concentration was from 54 to 62 percent. The small increase in CO conversion results from high enough permeation of reactant CO from feed gas side to permeate side, thereby not affecting the reaction equilibrium on the feed gas side significantly. Simulations

indicated that rapid permeation of product hydrogen with respect to CO is essential for shifting the reaction equilibrium significantly to increase CO conversion.

The current status of carbon membrane development is not sufficient to significantly increase CO conversion with hydrogen separation at high-pressure conditions. Also, a number of stages would be required with a corresponding decrease in overall hydrogen recovery to obtain product hydrogen concentrations in excess of 80 percent. A further increase in the gas separation ability of these membranes at high-pressure operation is thus needed to make such a concept technically feasible.

Future work in this area may be directed toward making the carbon membrane gas separation layer defect-free so as to minimize the viscous contribution seen at high pressure conditions. The carbon membranes need to be fabricated in a module for testing in an actual coal gas environment. WGS reaction experiments need to be conducted under high stage cut conditions using longer membranes to verify model predictions experimentally. Alternative approaches to Knudsen diffusion separation, based on molecular sieve-type carbon membranes, may be investigated to increase the hydrogen separation factors beyond the Knudsen diffusion limits.

SECTION 1

INTRODUCTION

In direct coal liquefaction processes, the production, efficient use, and recovery of hydrogen account for over 50 percent of the capital cost. Conventional hydrogen plants for coal liquefaction typically employ coal gasification followed by water-gas shift (WGS) reaction, complicated liquid-phase processing steps for acid gas removal, Claus/Scot sulfur recovery, and hydrogen separation (e.g., by pressure swing adsorption). These plants will not compete with natural gas-based hydrogen plants until the price of natural gas is increased to approximately $7.0 per million Btu (Bartis and Marks, 1984). Thus, for coal-gasification-based plants to be competitive, significant improvements are required in each processing step and/or a significant reduction is required in the number of processing steps.

This project aims to reduce the cost of hydrogen by combining the WGS reaction and hydrogen separation steps using a catalytic membrane reactor. The WGS reaction converts CO present in the gasifier gas streams to hydrogen by reacting the CO with steam as shown in Equation (1-1):

$$CO + H_2O \rightleftharpoons CO_2 + H_2 \; . \qquad (1\text{-}1)$$

The conversion of CO by this reaction in a typical coal gas environment is limited by chemical equilibrium. By continually separating hydrogen in the reactor, thermodynamic and kinetic limitations in the WGS reaction are reduced, leading to greater hydrogen production. The economics of the overall plant may be further enhanced by conducting the WGS step as well as other downstream steps at high-temperature high-pressure (HTHP) conditions.

Catalytic membrane reactors offer an inherent ability to combine reaction and product separation in a single operation. The membrane provides a selective removal of one or more products simultaneously with the reaction, so that the reaction equilibrium is continually shifted to increase product formation. To utilize such a concept, a hydrogen-selective membrane capable of operating at up to 20 atm and 300 to 500 °C is needed. In addition, such a membrane should be tolerant to various contaminants in gasifier gas streams such as hydrogen sulfide. At such conditions, currently available polymeric hydrogen-selective membranes, of course, cannot be used. The metallic palladium membranes are known to be hydrogen selective, but they would easily be degraded by the sulfur species in the gas stream.

Because of its low molecular weight, hydrogen may be separated selectively from other gases in the Knudsen diffusion regime. Knudsen diffusion occurs when the mean pore diameter of the membrane material is less than the mean free path of the gas molecule. At these conditions, gas species permeate independently of each other at a rate inversely proportional to the square root of their molecular weight. This mechanism thus will allow hydrogen to permeate about 3.7 times faster than carbon monoxide and nitrogen and will require a membrane with pore

sizes on the order of 10 Å to 20 Å. Inorganic microporous membranes such as ceramic and carbon with a permselective layer of appropriate pore size are thus possible candidates for membrane reactors for WGS reaction. Inorganic microporous membranes have been developed primarily for liquid filtration applications. A comprehensive summary of inorganic membrane developments has been prepared by Hsieh (1988), who also provides a review of small-scale gas separation studies and the associated separation factors achieved.

This project focuses on carbon composite microporous membranes. Carbon was chosen for its chemical inertness and tolerance for water and sulfur gases, better thermal expansion property compared to ceramic membranes, and the ease of surface modifications. A number of studies have been conducted on pyrolysis of organic polymer precursors, which can lead to porous carbons. The porosity and pore size of the carbons produced have been shown to depend upon pyrolysis conditions (Neely and Isacoff, 1982). The commercially available carbon composite tubular membranes by Carbone of America Corporation are produced by the pyrolysis of an appropriate thermosetting polymer such as polyacrylonitrile (PAN). A carbon support tube with very large pores is first prepared followed by the addition of a permselective layer to produce desired liquid filtration characteristics. These tubes provide the starting point for this project, which is aimed at modifying the membranes to make them more suitable for the catalytic membrane reactor application to maximize hydrogen production.

SECTION 2

LITERATURE REVIEW

A literature search was conducted initially to gather available information on polymer pyrolysis leading to carbon formation, catalysts for WGS reaction, and techniques for incorporating catalysts on carbon supports. The information on WGS catalysts was deemed adequate for direct use in this project. The search identified cobalt-molybdenum sulfide as a sulfur-tolerant WGS catalyst active in the applicable temperature range of 400 °C for this project. Techniques for preparing sulfide catalysts were identified for use in this project.

Much of the information on polymer pyrolysis was related to the production of activated carbon for adsorption; however, this information was useful for selecting suitable organic precursors for this project, which were chosen on the basis of their high carbon yield upon pyrolysis. Formation of carbon refers to basically three different types of materials, each of which can, in principle, be used as a catalyst support. These materials can be divided as follows: activated carbons, carbon black composites, and polymer-derived carbons (Abotsi and Scaroni, 1989; Walker, 1978).

Activated carbons are produced by heating various carbonaceous precursors (wood, coconut shell, etc.) in an inert atmosphere, followed by a controlled burnoff of a portion of the carbon using steam, air, or CO_2. The resulting material has a number of properties that make it useful as an adsorbent but limited its applicability as a catalyst support and membrane material. These properties include a high proportion of micropores (<2 nm), nonuniform surface properties, and the presence of varying amounts of inorganic impurities that may be catalytically active for undesired reactions. Because the usual procedure for preparing activated carbons is not likely to lead to a suitable defect-free membrane material, activated carbons were not considered in this project.

Carbon black composites are produced by the controlled pyrolysis of hydrocarbons such as methane to produce fine particles of carbon black, which are then mixed with a binder and further pyrolized. The result is a material with a more open and controllable pore structure than activated carbons without the attendant inorganic contaminants. The pore size of such composites depends on the carbon black particle size. The commercial carbon microfiltration membranes utilize fine carbon particles to produce the microfiltration layer. Thus, a similar procedure is not likely to produce the ultrafine pores of interest in this study.

The pyrolysis of polymer materials has been studied extensively and the literature indicates that it produces carbon materials of uniform properties. Pyrolyzed dense polymer membranes have been shown to exhibit molecular sieve-type membrane properties (Koresh and Sofer, 1983). Pyrolysis of a polymer is also used in the preparation of a support tube for the carbon microfiltration membrane. A detailed review of literature of such polymer-derived carbons is presented in Section 2.1. A large body of this literature pertains to production of carbon

adsorbents and carbon supports for catalysts; however, it also identifies possible polymer precursor candidates for the carbon membrane modifications.

2.1 Polymer-Derived Carbons

Polymer-derived carbons are prepared by the controlled pyrolysis of synthetic organic polymers such as sulfonated styrene/divinyl benzene or PAN (Hucke, 1975; Neely, 1981). Extreme pyrolysis of these materials can lead to graphite which, though not normally used as a catalyst support, has found some use as a support for cobalt/molybdenum catalysts (Stevens and Edmonds, 1979). A variation of polymer-derived carbons is the so-called glassy carbon, which is prepared by polymerization of a carbon-containing monomer in a solution of various dispersing and pore-forming agents (e.g., Hucke, 1975). These glassy carbons have a higher micropore (<2 nm) content than other polymer-derived carbon.

Because of the mechanical durability of polymer-derived carbons and their chemical purity, these carbon materials are of primary interest in this project. These polymer-derived carbons have several attributes that make them attractive as a membrane material and catalyst support, including high surface area and controllable pore size distribution (Abotsi and Scaroni, 1989; Fleming, 1988). Neely and Isacoff (1982) have discussed the properties of carbons obtained from pyrolysis of a number of precursors. The ability of the polymer precursors to fuse upon heating determines that polymer's ability to form a suitable porous membrane. The surface area and the pore structure are two important properties of a membrane-support material. The surface area of carbon supports can be changed by various heat treatments (e.g., Walker et al., 1980), although the pore structures of polymer carbons derived from different starting polymers under different pretreatment conditions and different pyrolysis conditions are remarkably similar (Neely and Isacoff, 1982).

One important advantage of carbon as a catalyst support discussed by Abotsi and Scaroni (1989) is its low coking potential compared to other supports such as alumina. The coking tendency is related to surface acidity. Preadsorption of Lewis bases such as pyridine on these acidic sites was shown to reduce coking propensity (Scaroni et al., 1984). Scaroni et al. (1987) also discuss the use of vapor phase ammonia treatment at 873 to 1173 K to incorporate nitrogen-containing groups on two surfaces of a polymer-derived carbon. The functional groups on the carbon surface determining the surface acidity are expected to play a role in determining the coking possibilities. One advantage of carbon as a catalyst support is that it can be treated to reduce or eliminate Brönsted acidity, thus reducing its coking tendency (Scaroni, 1981).

Another way the carbon surface properties can influence the catalytic activity is by promoting the adsorption of catalysts. Derbyshire et al. (1986) studied the effect of functional groups on the carbon surface on the catalytic activity of the carbon-supported molybdenum hydrodesulfurization catalysts. In their studies, functional O and N groups were incorporated by either partially oxidizing or nitriding the carbon surface. The effect of oxygen functional groups was inconclusive or negative. In contrast to preoxidation effects, prenitriding was found to distinctly enhance the catalytic activity. At the same time there was no commensurate increase

in the coking propensity. It was hypothesized by Derbyshire et al. (1986) that the increased activity may be related to the presence of nitrogen-containing surface groups, which provide preferential sites for the adsorption of Mo species.

The choice of an organic precursor might be quite important in determining catalytic activity and coking tendencies. Precursors leading to basic functional groups are expected to have lower coking tendencies. Nitrogen-containing precursors are likely to provide nitrogen functional groups that promote the catalytic activity of molybdenum. Carbon supports based on PAN may be expected to enhance catalyst activity as compared to that from polyvinyl alcohol, which contains oxygen groups. The heat treatment conditions of the polymers can also strongly affect the surface area of the resulting carbon. Some specific polymer-derived carbon preparation recipes that are relevant to this project are discussed in the following paragraphs.

Walker et al. (1966) showed that the nature of molecular sieving in polymer-derived glassy carbons could be altered, depending on the organic precursor, heat treatment temperature, and addition of activated carbon to the original mix. Schmitt and Walker (1971, 1972) used this concept to produce a shape-selective platinum catalyst on a carbon molecular sieve. A recipe of five parts partially polymerized polyfurfuryl alcohol (PFA) to one part activated carbon and a water solution of chloroplatinic acid was used. Following further polymerization of the PFA, the sample was charred at 700 °C.

Walker et al. (1977) utilized Hucke's patent (1975) to produce monolithic carbon supports in pellet form. A carbon-yielding compound (furfuryl alcohol [FA]), a liquid pore former (diethylene glycol [DEG] or polyethylene glycol [PEG]), a dispersing agent (Triton X-100 or PEG), and a polymerization catalyst (p-toluene sulfonic acid) were used. Following partial polymerization of the FA, the pore former was evaporated off leaving a narrow pore-size distribution of larger pores. Pore size could be varied by choosing different heat treatment temperatures.

Schmitt et al. (1976) described a patented technique for making carbon black polymer derived carbon composites with pores primarily in the 40 Å to 100 Å range. The technique consisted of dissolving 7.5 g of PFA in 75 cm^3 of acetone. Added to this solution were 30 g of carbon black particles having a mean diameter of 120 Å. After thorough mixing, the resulting composition was extruded. The extrudates were heated overnight at 100 °C to volatilize off the acetone present, then heated under flowing N_2 to 600 °C in 1 hour and held at this temperature for an additional hour. Cylindrical pellets of about 1/16th-in. diameter were obtained.

Scaroni et al. (1987) described another modification of the Hucke patent for producing polymer-derived glassy carbon. A solution of tetraethylene glycol (TEG), a liquid pore former, and Triton X-100, a dispersing agent, was made by heating the two liquids to 353 K followed by dissolution of a known quantity of paratoluene sulfonic acid (PTSA) (a polymerization catalyst) or nitric acid (HNO_3) in hot solution. The resulting solution was then cooled to about -5 °C to reduce the rate of the exothermic reaction, after which FA was added by drops. It was necessary to add the FA slowly in order to prevent a rapid, uncontrollable foamy reaction.

Following partial polymerization of the carbon-yielding monomer, the volatile components were expelled in two stages at 700 °C and 1,200 °C in a nitrogen environment. A 45 wt% carbon yield containing both macro and micro pores was produced.

Neely (1981) described the production of polymer-derived carbons based on pyrolysis of sulfonated styrene-divinyl benzene copolymer. A series of chemical reactions occurs which transforms the porous starting material into a carbon replica of the original plastic. Desired pore size distribution could be obtained by varying the heat treatment temperature (500 °C to 1,200 °C) in the 2.5 Å to 300 Å range.

The carbon composite membrane tubes produced by LeCarbone Lorraine in France, the parent company of Carbone of America Corporation, are produced by pyrolysis of PAN tubes in a controlled environment (Fleming, 1988). This yields a support tube of pores on the order of 10 μm. A layer of fine carbon particles is then deposited followed by controlled pyrolysis to produce pores of 2,000 Å suitable for microfiltration. In the current project, the challenge is to bring the 2,000 Å down to around 100 Å without a significant decrease in pore area.

Koresh and Sofer (1983) and Sofer et al. (1987) investigated pyrolysis of dense polymeric hollow fiber membranes to produce carbon molecular sieve-type membranes. Experiments were conducted by pyrolyzing cellulose hollow fiber membranes at 800 °C and 950 °C. Pyrolysis at higher temperatures was found to produce finer size pores in the membrane. The high-temperature pyrolysis in an inert atmosphere was found to produce pores of molecular dimensions. High-temperature activation of these membranes by an oxidant (typically air) opened up the pores. The activated membranes were shown to have higher permeation rates and lower selectivities similar to Knudsen diffusion separation. The polymer pyrolysis is of direct relevance to the current project.

2.2 WGS Catalysts

An excellent review of the WGS catalysts prepared by Newsome (1980) indicates three major categories of these catalysts: (1) high-temperature (up to 550 °C) iron-based catalysts; (2) low-temperature (175 to 205 °C) copper-based catalysts; and (3) medium temperature (350 to 450 °C) sulfur-tolerant cobalt-molybdenum-based catalysts. In the current application an effective catalyst should withstand moderate to high temperatures of 300 to 500 °C and high levels of sulfur species (primarily H_2S) in the coal gas. The copper-based catalysts are easily poisoned by sulfur and also are effective only at low temperatures and thus may be eliminated from further consideration.

The iron-based catalyst has been shown to be tolerant to low levels (less than 500 ppm) of sulfur in the gas phase (Bohlbro and Jorgensen, 1970); however, its activity decreases approximately in proportion to the square root of the sulfur concentrations at higher levels. Iron-chromium catalysts are by far the most commonly used catalysts and usually consist of 74 percent Fe_2O_3 (Sherwood, 1961). The optimum concentration of Cr_2O_3 has been found to be about 14 percent (Markina et al., 1961). It is generally believed that chromium acts as a

stabilizer rather than a promoter and prevents high temperature sintering and loss of surface area. Information on the proven "ferrochrome" catalyst is reviewed by Newsome (1980). Because the iron catalysts are susceptible to deactivation at high sulfur levels, they should be considered only if the other reportedly sulfur-tolerant catalysts are not found to be feasible. Carbon-supported iron-sulfide catalysts for hydrodesulfurization reactions have also been reported (Ramselaar et al., 1989), though their activity for the WGS reaction is not known.

Newsome (1980) discusses a family of "completely sulfur-tolerant" catalysts that incorporate single or mixed metals of Groups VI and VIII (other than Fe and Cr) generally supported on alumina. Very often alkali promoters are added and the catalysts are partially or completely sulfided. Examples include: Mo-MgO (Tsuchimoto et al., 1968), Ni or Co with Mo (Prins et al., 1989; Levinson et al., 1974; Tsuchimoto et al., 1968; Morita and Tsuchimoto, 1967; Newling and Rich, 1966; Harris, 1964), Ni, Mo, or Co sulfides (Newling and Rich, 1966; Reitz and Lorenz, 1963; Wustrow et al., 1954), Co/Mo/Ni with alkali promoters, and Co-Mo with added alkali (Overstreet, 1974; Berispek, 1975; Aldridge and Kalina, 1971; Segura et al., 1976; Riley and Aldridge, 1977).

This last catalyst, promoted with various cesium and potassium compounds, is completely sulfided in its most active form. Overstreet (1974) compared its activity (in a sulfided form) with both iron- and copper-based commercial shift catalysts. He found it to be more active than either commercial catalyst. Further work at the same laboratories by Berispek (1975) examined the effect of other alkali promoters (Li, Na, K, and Li plus Cs) on the same catalyst. The K-impregnated catalyst was even more active than the Cs-impregnated catalyst of Overstreet (1974).

An oxide catalyst, which is claimed to be "completely sulfur tolerant" was recently reported by Czech scientists (Kettman et al., 1988). Building on the results of Newsome (1980), this catalyst is a modification of a Co-Mo/Al_2O_3 hydrodesulfurization catalyst, to which K_2CO_3 is added to form a K-Co-Mo/Al_2O_3 WGS catalyst after calcination. This type of cobalt molybdate catalyst has been the subject of numerous patents for the WGS reaction in sulfur-containing gases. Hippo et al. (1979) also showed that the shift reaction rate was proportional to the calcium content of coal char. This, together with the work of Kettman et al., suggests that alkali-promoted oxide catalysts, including K-Co-Mo/Al_2O_3, may be of interest. Another important aspect influencing catalyst activity is the addition of alkali metals such as potassium and cesium. Overstreet (1974) and Berispek (1975) have made extensive studies of the Co-Mo catalysts with the addition of alkali compounds; their studies should provide an excellent base for any further studies on these types of catalysts.

The WGS molybdenum catalysts (along with cobalt or tungsten) are also widely used for other processes such as hydrodesulfurization, e.g., that of thiophene (Abotsi and Scaroni, 1989; Ohtsuka, 1977; Owens and Amberg, 1961; Grange, 1980; and Furimsky, 1980). In these applications also, the catalysts are in the form of sulfides. Almost all of these studies on sulfur-tolerant species indicate that the sulfide is the active form of the catalysts, and any catalyst initially present as an oxide is eventually sulfided with enhanced reactivity.

Catalyst activity depends mainly on physical properties and chemical composition. The properties of importance are physical and metal oxide surface area, pore volume, and pore size distribution. In addition, their physical incorporation in the porous carbon support will also be extremely important. The chemical composition in terms of the atomic ratio of cobalt, molybdenum, and any added alkali will have a substantial effect on the catalyst properties. Typically a Co:Mo ratio of 1:4 has been used (Berispek, 1975). Because of the known success of the Co-Mo catalyst in a sulfur environment, initial experimental studies should focus on this family of catalyst with selected alkali additives. The properties strongly depend on the method of preparation, which is discussed in the next section.

2.3 Synthesis of Carbon-Supported WGS Catalysts

There are basically two ways to prepare such carbon-supported WGS catalysts:

- Prepare catalysts as part of the precursor of the carbon membrane.
- Impregnate the carbon support. This can be done by three separate approaches:
  - Gas phase adsorption,
  - Passing a solution containing the metal precursors over the support (Butterworth and Scaroni, 1985), and
  - Incipient wetness.

These techniques are outlined by Abotsi and Scaroni (1989); Walker (1962); and Butterworth and Scaroni (1985).

Incipient wetness appears to be the method of choice for many systems. Incipient wetness consists of preparing an aqueous solution containing the metal precursors and bringing it into contact with the support. Only sufficient solution is prepared to impregnate the solid to the desired metal loading. Physically, this consists of calculating the metal loading on the catalysts and, knowing the pore volume of the support, preparing a solution equal to the pore volume of the support with a concentration of metals equal to the desired metal loading. Typical loadings for cobalt/molybdenum catalysts, based on the cobalt/molybdenum sulfides, which are subsequently sulfided, are in the range of 1 to 3 percent by weight cobalt and a cobalt to molybdenum ratio of 1:2 up to 1:4. For catalyst preparation on tubular membranes, however, impregnation using a flow-through approach would be more appropriate and practical. For the flow-through approach, impregnation time can be deduced using a standard equation for flow-through capillaries. Aqueous solutions of the metal salt are prepared by dissolving ammonium heptamolybdate in an aqueous solution. The cobalt salt can be cobalt nitrate (Kotera et al., 1976) or cobalt acetate. Another precursor for molybdenum is ammonium paramolybdate (Kotera et al., 1976; Oades et al., 1989). An interesting modification to this procedure is the addition of 10 percent ethanol (i.e., ammonium heptamolybdate is dissolved in a solution of 90 percent water and 10 percent ethanol). This ethanol addition (Derbyshire et al., 1986) is said to be necessary

to assist in wetting the carbon surface, which is somewhat "hydrophobic." The weakly hydrophilic nature of GFT's membranes may make this unnecessary.

After impregnation, the catalysts are normally dried, either in the air or in nitrogen, followed by decomposition of catalyst precursors by calcination at temperatures of 500 to 650 °C (Oades et al., 1989; Brinen and Armstrong, 1958; Owens and Amberg, 1961). Oades et al. (1989) also discuss reduction of the catalyst by immersion in flowing hydrogen at 450 °C for approximately 16 hours. For carbon-supported catalysts, calcination in air is out of the question. For these catalysts, activation may be accomplished by heating in an inert or in a reducing gas as done by Oades et al. Sulfidation, as a key step, is discussed in some detail in the following paragraph.

Sulfidation can be accomplished in one of three ways. One way would be to pass H_2S, H_2S/H_2 mixture, or other light sulfur gases mixed with H_2 over the dried calcined catalyst. It may be possible to accomplish sulfidation with H_2/H_2S treatment without prior calcination. Derbyshire et al. (1986) discuss an interesting technique for sulfidation. The solution used to impregnate the catalysts was saturated with H_2S at room temperature to form an ammonium salt. In this case, the active catalyst was produced in situ, eliminating the need for gas-phase sulfiding. This may have the advantage of avoiding changes in the carbon or catalyst surface caused by air drying. The use of an H_2S-saturated solution of ammonium salt to produce the sulfided catalysts may require repeated impregnations and drying in vacuum at 100 °C between each step to produce the required loading (Derbyshire et al., 1986). Repeated impregnation may be necessary to obtain metal loadings approaching 15 wt% (Scaroni et al., 1987). Another possibility of obtaining sulfide catalysts is to use thiomolybdate compounds for impregnation, followed by reduction in a stream of hydrogen at temperatures between 400 and 450 °C (Abotsi, 1987; Kolboe and Amberg, 1966). To use this approach for cobalt and potassium, of course, suitable thio compounds must be available. Some specific catalyst preparation techniques and other important points are discussed below.

Topsoe et al. (1979) prepared a cobalt molybdate catalyst on a support identified only as "active carbon" by impregnation with an ammonia solution of cobalt nitrate and ammonium paramolybdate. This catalyst was dried in air at 230 °C for 24 hours and sulfided in a 2 percent H_2S stream (in hydrogen) at 325 °C for 24 hours.

Potassium-promoted cobalt molybdenum catalysts, which may be of interest based on other literature, are prepared by dissolving potassium acetate in ethanol and adding the appropriate quantity of this acetate/ethanol solution to the dried carbon catalyst and then recalcining in nitrogen at 500 °C for 10 hours (Oades et al., 1989).

Preparation of catalysts other than cobalt/molybdate are discussed by Chatwick et al. (1983) and Merango et al. (1983). These involve, respectively, P-Ni-Mo/γ-Al_2O_3 and tungsten-molybdenum on alumina. Urban and Albert (1973) described the preparation of a cobalt/molybdenum sulfide catalyst on activated carbon. Their catalyst was prepared by impregnation of 10/30 mesh particles of activated carbon with an aqueous solution of cobalt acetate resulting in a final catalyst loading of 4.6 wt% cobalt oxide. Impregnation is done at

room temperature for 30 minutes. The excess solution was evaporated in a rotary at 105 °C for 1 hour. The dried composite was then placed in a closed vessel, evacuated to 30 mm, and contacted with pure hydrogen sulfide. The hydrogen sulfide was used to bring the evacuated vessel up to atmospheric pressure. This was repeated three times until the composite did not absorb any more H_2S. This was then purged with pure nitrogen at room temperature and atmospheric pressure until less than 1 ppm of H_2S was present in the purged gas. This composite was then impregnated with an aqueous solution of ammonium hydroxide and molybdic acid to result in a final catalyst of 2.3 percent molybdenum oxide. Molybdenum was impregnated in the same way as cobalt. The resulting bimetallic catalyst was dried and sulfided just as before, i.e., in a vacuum apparatus using H_2S.

Venter et al. (1987) discussed the pretreatment of an amorphus commercial carbon by treatment in hydrogen at 1,223 K for 12 hours to remove the sulfur apparently inherent in the carbon. This carbon was also treated at 573 K under vacuum of 10^{-4} kPa for 8 hours to remove the physisorbed water. This may be necessary if sulfur or water in the carbon itself is found to inhibit either impregnation or metal dispersion.

Daly and Brinen (1987) described the pretreatment of carbon supports with ammonia prior to the preparation of a cobalt molybdenum oxide catalyst. These ammonia-treated carbons apparently exhibited enhanced activity for hydroconversion of asphaltene molecules in this study. The ammonia pretreatment was done first by heating the carbon in nitrogen to 900 °C. Next the inlet nitrogen stream was diverted to a bubbler containing concentrated ammonium hydroxide (28 percent), and the ammonia/nitrogen stream was passed over the carbon at a rate of 1 L/min for 2 hours. The ammonia-treated material was then cooled to room temperature in nitrogen. This resulted in a carbon containing about 4 percent nitrogen. Cobalt/molybdenum oxide catalyst was then prepared from this ammonia-created carbon using the incipient wetness technique. This consisted of first impregnating the carbon with an aqueous solution of ammonium heptamolybdate, drying it at 120 °C, and impregnating it then with an aqueous solution of cobalt nitrate, followed with a second drying at 120 °C, heat treating in nitrogen at 400 °C for 1 hour, resulting in a cobalt/oxide molybdenum/oxide catalyst on carbon.

SECTION 3

CARBON MEMBRANE MODIFICATION

3.1 Carbon Composite Microfiltration Membranes

Carbon composite microfiltration membranes are commercially available in the United States from Carbone of America Corporation and are made by LeCarbone Lorraine. The commercial carbon membranes have pore sizes in the range of 0.1 to 1.0 μm and are used for liquid microfiltration applications. The pore size must be reduced considerably to make these membranes suitable for gas separation applications. Figure 3-1 shows the schematic of a modified carbon membrane structure. The membranes have a tubular geometry with a 6-mm nominal internal diameter and 8-mm outside diameter with a thickness of 1 mm.

The commercial membranes are produced by the pyrolysis of an appropriate thermosetting polymer such as PAN. A support tube is first prepared composed of woven carbon fibers. A liquid microfiltration layer of small carbon particles is then added on the inside of the tube to provide desired microfiltration characteristics. The membrane surface is weakly hydrophilic and has a high porosity (65 to 75 percent) and low tortuosity. The membrane tubes have a bursting pressure of 1,500 psi and have been used successfully in corrosive liquid environments.

Two grades of commercial carbon membranes were obtained from Carbone of America Corporation for this project: 0.2 μm and 1.0 μm. The membrane samples were analyzed by mercury porosimetry, BET surface area analysis, scanning electron microscopy (SEM) analysis, and permeation studies. A small permeation cell was constructed to house a 2-1/2-in. long carbon membrane tube for low-temperature permeation studies. The 8-mm O.D. carbon tube was connected to 1/4-in. stainless steel tubing using an 8-mm to 1/4-in. reducer and Teflon ferrules on the carbon tube. In addition, the joints were sealed by silicone sealant. Pure component permeation rates were obtained by maintaining a constant pressure of the pure component inside the tube and measuring the permeation flow rates by a soap bubble meter, as shown in Figure 3-2.

3.1.1 Mercury Porosimetry

The carbon tube samples were analyzed using Micromeritics mercury porosimeter (Model Autopore II 9220). This porosimeter is capable of operating at pressures up to 60,000 psia and thus is able to detect pores down to 30 Å (3 nm) in size. The typical pore size distributions obtained using this instrument for the 0.2-μm and 1.0-μm tubes are shown in Figures 3-3 and 3-4, respectively. These figures indicate similar pore size distributions for both types of tubes with a primary peak between 1 and 4 μm. The median pore diameter of the 0.2-μm tube was about 2.1 μm, whereas that for the 1.0-μm tube was about 2.7 μm. Because of poor resolutionin the fine pore range, this technique is not likely to identify changes in the membrane pore size distribution in the fine pore range as a result of membrane modification.

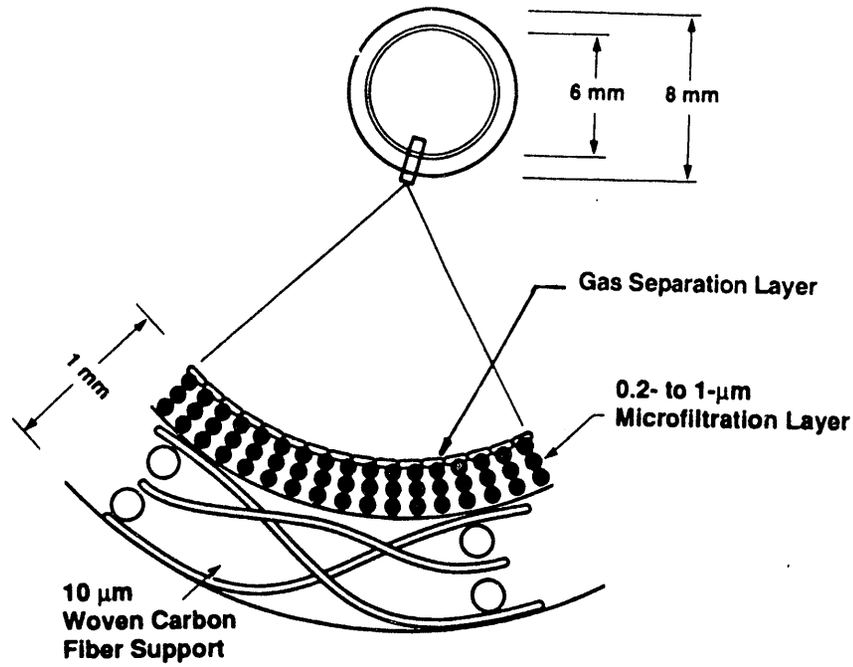

Figure 3-1. Schematic of carbon composite membrane structure.

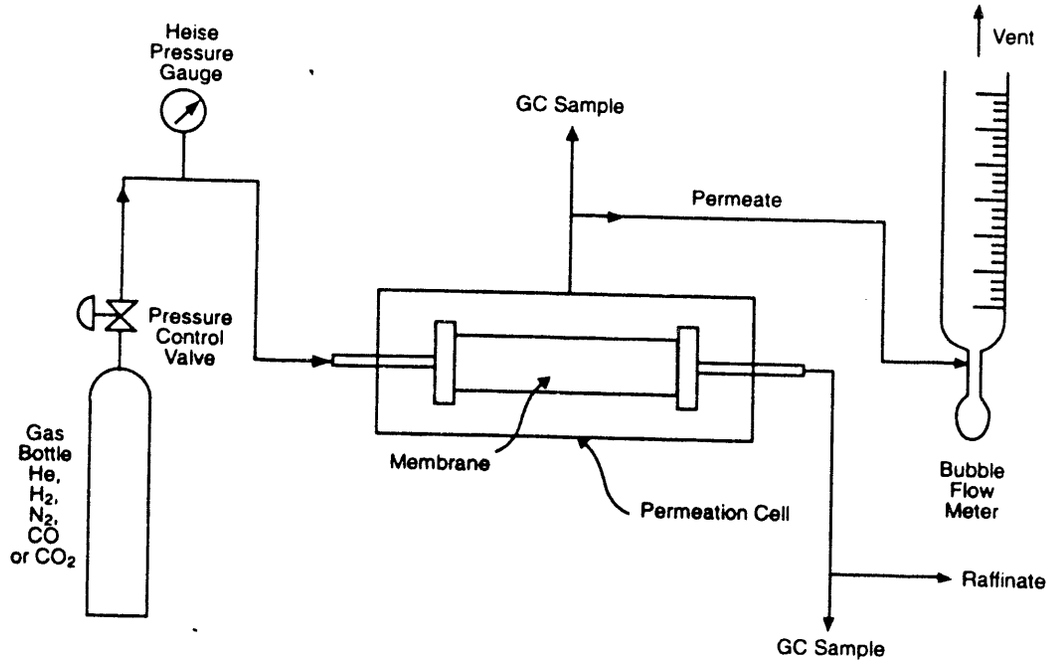

Figure 3-2. Schematic of a permeation cell test apparatus.

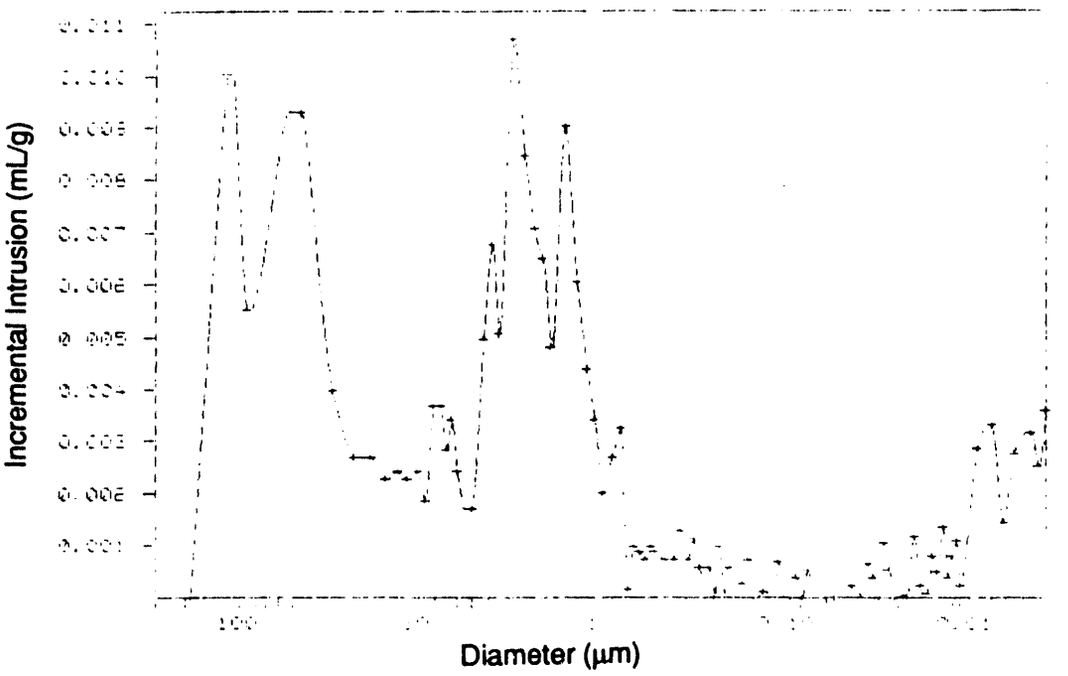

Figure 3-3. Pore size distribution for a 0.2-µm unmodified carbon membrane sample.

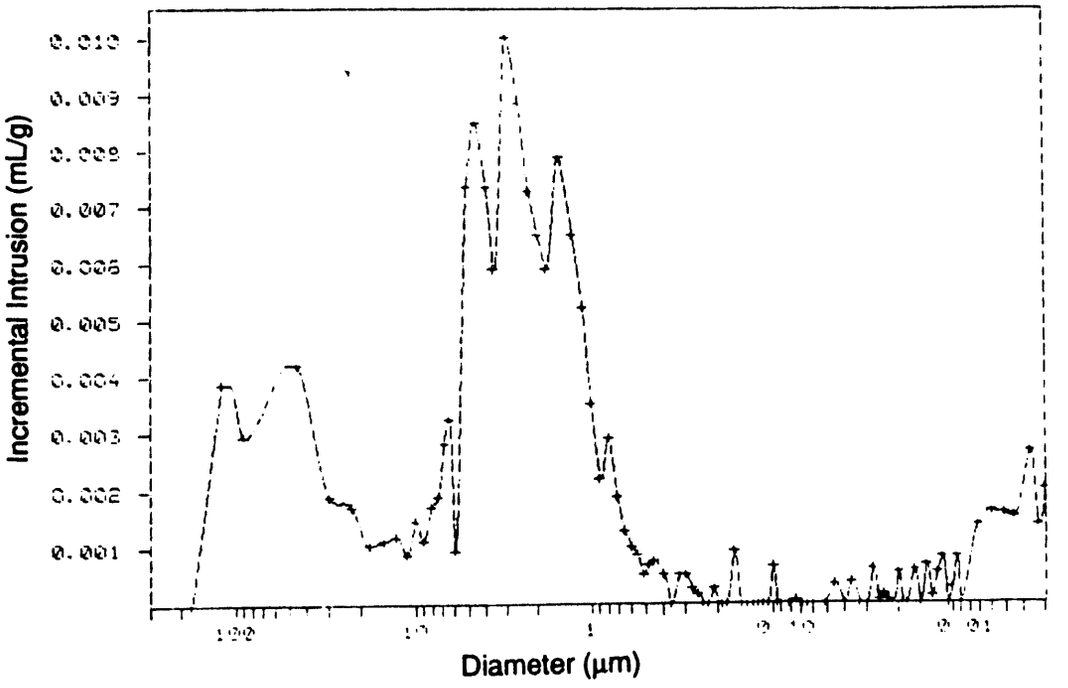

Figure 3-4. Pore size distribution for a 1.0-µm unmodified carbon membrane sample.

3.1.2 BET Surface Area Analysis

The surface area of the tube samples was determined using a QUANTASORB surface area analyzer by Quantachrome Corporation. Unlike the pore size distribution, the surface area analysis indicated a large difference in the two types of samples. The average surface area for an earlier batch of 0.2-μm tubes was found to be 14 m^2/g and for a later batch to be 10.1 m^2/g. The average surface area for the 1.0-μm tube was found to be 0.6 m^2/g. The bulk of the carbon tubes supplied by Carbone of America Corporation are composed of relatively nonporous interwoven carbon fibers, with a thin permselective porous layer deposited on the inner surface of the tubes. The large difference in the surface areas for similar pore size distributions thus indicates distinctly different structures of the porous layer deposited on the inner surface of the carbon tubes. This indication was further confirmed by the SEM analysis of the samples. Due to a very small expected weight change in the membrane modification process, the surface area analysis is also not likely to resolve adequately any structural changes during membrane modifications.

3.1.3 SEM Analysis

The carbon tube samples were analyzed using a Hitachi 800 Scanning Electron Microscope to determine the thickness, structure, and pore size distribution of the porous layer. The SEM analysis revealed distinctly different structures of the porous layer as indicated by the above-mentioned analyses. Figures 3-5 and 3-6 indicate the structure of the porous layers of the 0.2-μm and 1.0-μm tubes, respectively. Figure 3-7 shows the structure of more recent samples of the 0.2-μm tube. As Figure 3-5 indicates, the porous layer in older samples of a 0.2-μm tube appears to be composed of agglomerates of approximately 0.2-μm spherical particles. Although the particles themselves are small, the aggregates appear to have comparatively bigger channels of 1 to 2 μm, confirming previously obtained pore size distribution. Figure 3-6, on the other hand, indicates much coarser fused structure for the 1.0-μm tube porous layer, with channels of 1 to 3 μm. The newer samples of the 0.2-μm tube show a structure similar to the 1.0-μm tube except for smaller pore sizes. The grainy structure of the porous layer in the 0.2-μm tube as compared to that for the 1.0-μm tube can explain the observed high surface area for the 0.2-μm tube samples. The observed thickness of the porous layer in the 0.2-μm tube was approximately 12 μm, whereas that for the 1.0-μm tube was about 18 μm.

3.1.4 Permeation Cell Studies

Figure 3-2 shows the schematic of the experimental setup used to determine the permeation flux rate through an approximately 2-in. section of a carbon tube sample. All experiments were conducted at approximately 20 °C and at pressure differentials across the tube up to 760 mm Hg with a downstream pressure of 1 atm. Experiments were conducted with pure hydrogen, helium,

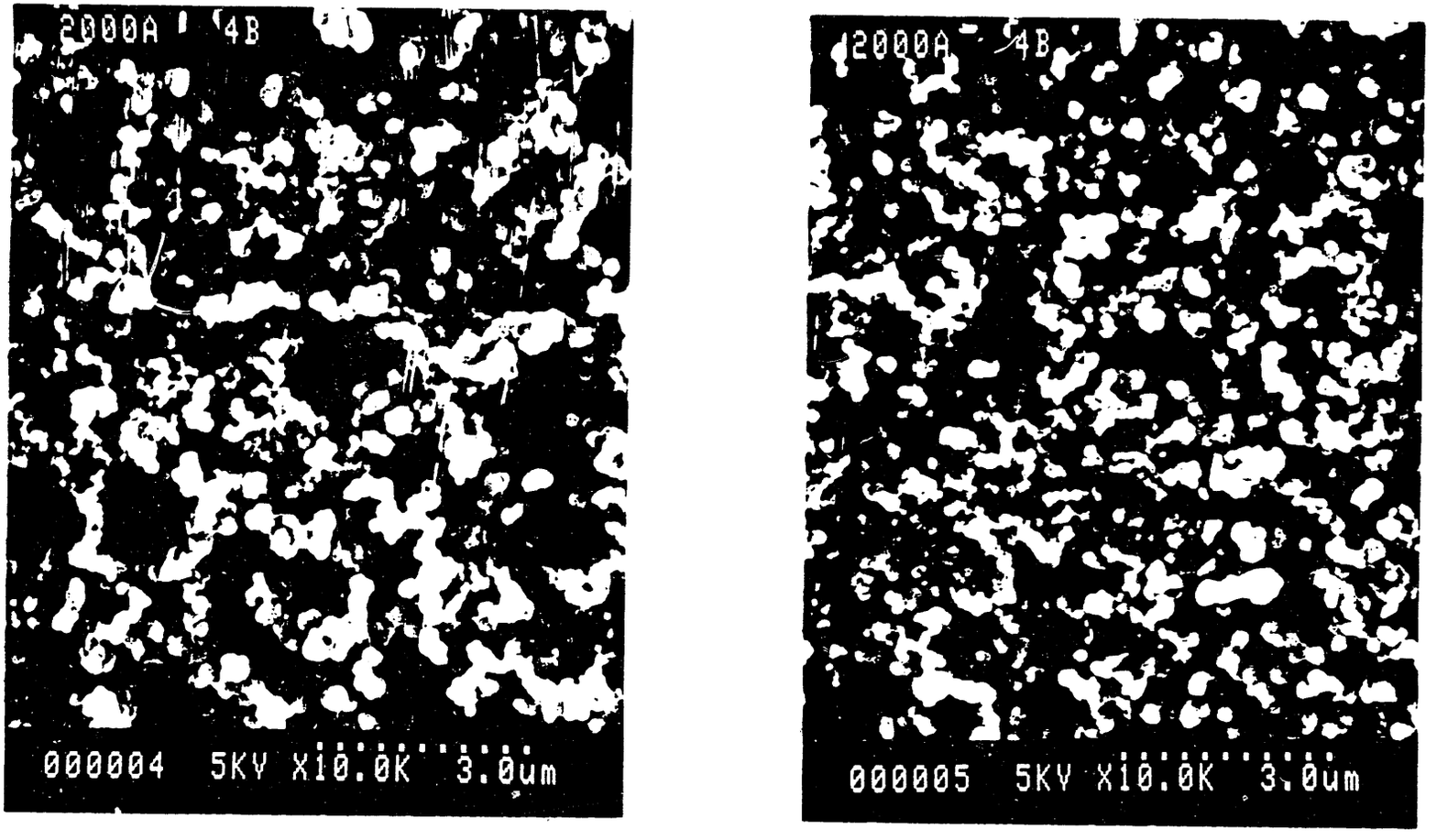

Figure 3-5. Scanning electron micrograph of a 0.2-μm unmodified carbon membrane sample.

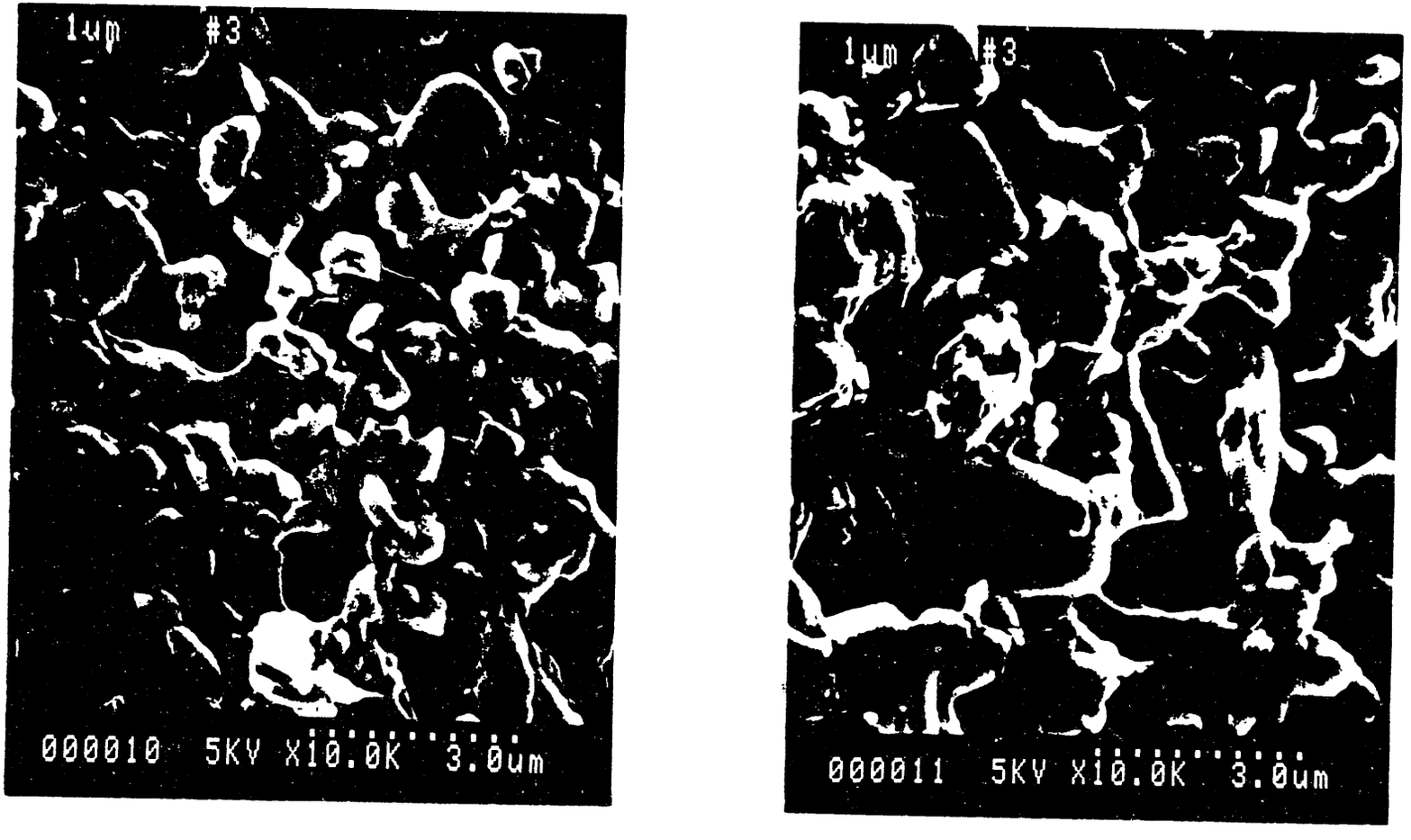

Figure 3-6. Scanning electron micrograph of a 1.0-µm unmodified carbon membrane sample.

Figure 3-7. Scanning electron micrograph of a 0.2-µm unmodified carbon membrane sample (recent batch).

nitrogen, carbon monoxide, and carbon dioxide gases. The flux rate through a porous membrane was correlated by the following expression:

$$Q = \frac{K A}{L} \Delta P \qquad (3\text{-}1)$$

where

Q = flux rate, cm^3/s
K = permeability, $(cm^3/s)\cdot cm^2\cdot$mm Hg
A = membrane surface area, cm^2
L = membrane layer thickness, cm
ΔP = pressure differential across membrane, mm Hg.

The collected data were analyzed using the above equation to determine the permeability of the two unmodified carbon tube grade samples for the five different gases used, and the results are presented in Table 3-1. As seen from this table, the permeability of the 1.0-μm tube was greater than that for the 0.2-μm tube. Both tube samples indicated permeability with respect to hydrogen to be greater by a factor of two or more when compared with the permeabilities with respect to nitrogen or carbon dioxide.

Table 3-1. Permeability of Unmodified Carbon Membrane Tubes for Various Gases

	Permeability ($cm^3/s\cdot cm^2\cdot$mm Hg) x 10^3	
Gas	0.2 μm	1.0 μm
H_2	6.7	15.8
He	3.9	8.3
N_2	2.6	7.1
CO	2.6	7.1
CO_2	2.6	7.7

The permeation studies provide the most direct measure of the effectiveness of membrane modifications in changing the gas separation properties of the carbon membranes, whereas other techniques can at best provide an indirect qualitative indication of the effectiveness of membrane modifications. Therefore, the effectiveness of the membrane modification technique was evaluated primarily using the direct permeation studies.

3.2 Membrane Modification Approach

The pore size of the unmodified carbon microfiltration membranes is too large to be effective for gas separation applications. Porous membranes may separate gases based upon differences in permeation rates for different gas species. Four different mechanisms are possible to achieve gas separation using porous membranes: molecular sieving, Knudsen diffusion, surface diffusion, and capillary condensation.

One obvious mechanism of gas separation by such passive membranes is size exclusion or molecular sieving; however, to take advantage of this mechanism the pore size needs to be very small (on the order of 3 to 5 Å, i.e., 0.3 to 0.5 nm). Such a small pore size reduces the permeability substantially. In order to be selective for a specific gas, the membrane pore size also needs to be controlled in an extremely narrow range. Tailoring of a membrane to such specifications in a reproducible manner is difficult.

Knudsen diffusion occurs when the pore diameter is significantly less than the mean free path of the gas. This allows each gas species to permeate individually at a rate inversely proportional to the square root of the molecular weight. This relationship has been demonstrated in literature, e.g., by Havredaki and Petropoulos (1983) with compacted silica and alumina membranes and by Lee and Khang (1986) with pyrolyzed rubber (silica) membrane. Knudsen diffusion will thus allow hydrogen to permeate four times faster than oxygen and will require pore sizes on the order of 100 Å (10 nm) or less. The mean free path of gas molecules is inversely proportional to the gas pressure. Thus even smaller size pores are needed at high gas pressures to separate gases by the Knudsen diffusion mechanism. Table 3-2 lists the mean free path of four common gases in a coal gasification environment at ambient conditions as well as at HTHP gasifier conditions. For dominant Knudsen diffusion separation at HTHP conditions, the membrane pore size needs to be on the order of 1 nm.

Table 3-2. Mean Free Path of Gas Species

	Mean free path, nm	
Species	**20 °C, 1 atm**	**400 °C, 20 atm**
H_2	122.4	15.9
N_2	65.1	9.0
CO	65.1	8.9
CO_2	42.1	6.7

Surface diffusion is important when one component is preferentially adsorbed on the surface. The type of adsorption is physisorption rather than chemisorption and occurs up to the boiling point of the adsorbed gas. As the adsorbed component accumulates on the pore surface, it diffuses faster than the other nonadsorbed components, thus causing separation of the gas mixture. Since physisorption decreases with increase in temperature, the utility of this mechanism for gas separation at high temperatures is questionable. At high pressure and low temperatures, certain gas species may undergo capillary condensation and form a liquid phase in the pores. When other gas species do not dissolve in the condensed species, they are excluded by the membrane, thereby affecting separation of the condensible species. Kameyama et al. (1979) separated H_2S from H_2 using this mechanism where H_2S condensed in the membrane pores and diffused across the membrane while blocking H_2 permeation. Barrer (1965) similarly separated SO_2 from H_2. Capillary condensation, of course, requires conditions under which condensation would be possible.

Capillary condensation and surface diffusion can occur at temperatures up to the boiling point of the species of interest. The high temperature conditions of the gasification gas streams

thus preclude most of the gases in these streams from being separated by these two mechanisms. The likely separation mechanisms with passive inorganic membranes would thus be Knudsen diffusion and molecular sieving in the coal-gas environment. Both of these mechanisms depend directly on the pore size distribution of the gas separating layer.

The molecular sieving mechanism can provide highly selective gas separation but would require pore size distribution to be in an extremely narrow pore size range. Such narrow and controlled size distribution is difficult to achieve and would also lead to very small gas flux rates. Thus, in this project, emphasis is placed on reducing membrane pore size to promote Knudsen diffusion, which can provide a limited gas separation based on its molecular weight. For H_2:CO_2 and H_2:CO separation of interest in a gasification environment, maximum separation factors of 4.7 and 3.7, respectively, may be expected for Knudsen diffusion separation.

The approach taken in this project to achieve the desired pore size reduction was to deposit an organic polymeric layer on the existing microfiltration layer followed by controlled pyrolysis to convert the polymer into carbon. During the coating process the existing pore network is expected to be covered and partially filled by the polymeric precursor. Subsequent pyrolysis is then expected to open up the closed pore network with a different pore size distribution.

3.3 Polymeric Precursors

In order to pyrolyze a polymer layer without deforming the deposited layer, the polymer needs to have thermosetting properties. Such polymers do not fuse or melt when heated and thus retain structural shape during heating and pyrolysis. Several thermosetting polymers are available as possible candidates for carbon formation as identified by Neely and Isacoff (1982). Polymer precursors were selected in this project on the basis of high carbon yield and include PAN, PFA, phenol-formaldehyde resin, cellulose, and furfuryl alcohol-phenolic (FAP) resin.

The polymer precursors chosen have high carbon content as well as high carbon yield upon pyrolysis: PAN has a carbon content of 67.9 percent with a reported net carbon yield upon pyrolysis of 51.6 percent, similarly PFA, phenol-formaldehyde resin, and FAP resin have net carbon yields of about 50 percent of the solids weight.

PAN, PFA, phenol-formaldehyde resin, and cellulose precursors were used in this project directly in their polymeric form and were applied by simple dip-coating. In some runs a coating of PAN was obtained by plasma polymerization of the acrylonitrile monomer. FAP resin was polymerized in situ by first applying a monomer solution and then activating polymerization in situ chemically. Each of these polymers required a certain procedure for curing and pyrolysis depending on the polymer structure and properties.

In addition to these polymeric precursors, the use of gas-phase pyrolysis of propylene to deposit a layer of carbon directly on the membrane was investigated. This process may be considered to be gas-phase adsorption/pyrolysis in one step. The general procedures followed with each of these precursors are described in the following paragraphs.

PAN: Numerous coating tests were conducted with PAN, because this polymer is used in manufacturing the microfiltration carbon membrane by LeCarbone Lorraine. PAN fibers were used as a source of this polymer. PAN is soluble in dimethyl acetamide (DMAC) solvent. Four concentrations of 1.25, 2.5, 5, and 10 percent PAN in DMAC were used for coating studies. Multiple coatings with intermediate drying were made to increase polymer loading on carbon tubes. The final coatings were vacuum dried overnight. Coated samples were first heated in air at 90 °C for 1 hour to complete the drying and shrinkage and then heated at 250 °C in air for 5 hours to complete the PAN cyclization process. The coated tubes were then pyrolyzed in nitrogen in stages up to 750 °C. Rapid and slow pyrolysis sequences were used with some pyrolysis runs conducted at 500 °C. Some coating studies were also conducted with recoating and pyrolyzing of previously coated and pyrolyzed samples. Samples were also prepared by the plasma polymerization process in which the acrylonitrile monomer was polymerized in the radio-frequency-induced plasma and the polymer (presumably PAN) was simultaneously deposited on the inner surface of the carbon tube.

PFA: PFA of 150,000 molecular weight was obtained from Polysciences, Inc. Solutions of PFA were prepared in acetone to obtain 10, 20, 30, and 40 percent PFA concentrations. Multiple coatings with intermediate drying were made to increase polymer loading on carbon tubes. The final coating was dried overnight in ambient air. Coated samples were heated in air at 100 °C to complete drying and then pyrolyzed in N_2 in stages up to 750 °C.

Phenol-Formaldehyde (Phenolic) Resin: Samples of this phenolic resin were obtained from Occidental Chemical Corporation's Durez Division. This resin has limited solubility in acetone and approximately 20 percent concentration solution was prepared. Again multiple coatings with intermediate drying were used to increase loading of the resin on carbon tubes. The coated tubes were air dried overnight and then cured in air at 150 °C for 1 hour. The cured coatings were then pyrolyzed in nitrogen in slow sequence up to 500 °C.

Cellulose: Cellulose powder obtained from Polysciences, Inc., was dissolved in DMAC using lithium chloride promoter, and a 3 percent solution of cellulose was obtained. Multiple coatings were used and the coatings were observed to be flaky. The coated samples were pyrolyzed in nitrogen starting at 100 °C and slowly increasing the temperature to 500 °C.

Propylene: High-temperature thermal pyrolysis of organic gases such as propylene can produce fine carbonaceous particles that may be deposited on different substrates. The conditions under which pyrolysis of propylene results in deposition on the carbon tube substrate were first investigated indicated that a temperature of up to 800 °C would be needed to produce significant weight gain of the carbon tube due to deposition of pyrolysis products. A sample of carbon tube was prepared by carrying out propylene pyrolysis until a 7.5 percent weight gain was obtained.

FAP Resin: Samples of this resin were obtained from QO Chemicals, Inc. Different grades of these resins are available based on viscosity and application. The viscosity of these resins can be varied by diluting them with FA. In situ polymerization of this resin is activated by a variety of acidic catalysts and the resin continues polymerizing to solidification. The resins were first applied by dip coating and then activated chemically. After air drying and complete

solidification, the coatings were first cured by heating them up to 150 °C and then were pyrolyzed in nitrogen up to 600 °C.

3.4 Pure Component Permeation Tests

Pure component permeation rates for all membrane samples were measured using the system shown schematically in Figure 3-2. All pure component permeation experiments were conducted at ambient conditions of approximately 20 °C and with pressure differentials across the membrane sample up to 760 mm Hg with a downstream pressure of 1 atm. Permeation rates were measured for H_2 and N_2 for all samples and for He, CO, and CO_2 for selected samples. The observed permeabilities expressed as std $cm^3/(s \cdot cm^2 \cdot mm\ Hg)$ for different membrane samples are shown in Table 3-3. Table 3-4 shows the ratios of observed hydrogen and nitrogen permeabilities. Although the decrease in permeation rates with membrane modification indicates overall porosity reduction, the increase in hydrogen-to-nitrogen permeability ratio indicates a decrease in pore size. For unmodified 0.2-μm carbon membrane tube this ratio was found to be about 2.5. For a completely Knudsen diffusion-dominated flow process, this ratio is expected to increase to about 3.7. These two parameters together thus indicate the effectiveness of the membrane modification process studied. The results for each of the precursors studied are discussed below.

PAN: The low concentrations of 1.25, 2.5, and 5 percent PAN solution were used for better penetration of the microfiltration membrane layer. However, the results in Tables 3-3 and 3-4 for these samples indicate increased flux rate and reduced H_2/N_2 permeation ratios. The coating prepared with 10 percent PAN solutions decreased the flux rates but did not increase the hydrogen-to-nitrogen permeation ratios significantly. By recoating a previously coated sample, the H_2/N_2 permeation ratio increased moderately to 2.74; however, it was still below the value of 3.7 expected for a diffusion-dominated process. The samples prepared by plasma polymerization of acrylonitrile also did not appear to improve the permeation characteristics significantly. The SEM analysis of some of the PAN-coated membrane samples indicated cracking of the coated layer as a possible problem that most likely occurred during pyrolysis. During cracking, the polymer layer was seen to lift the underlying microfiltration layer, which might explain the higher flux rates observed for some samples compared with the unmodified membrane.

PFA: Membrane samples were prepared with 10, 20, and 40 percent PFA concentrations in acetone. All samples were found to reduce the permeation rates but were also seen to decrease the hydrogen-to-nitrogen permeation ratios. The decrease in permeation rate was greater for higher concentration PFA solutions indicating pore blocking. However, the pore size distribution appears to become coarser as indicated by the reduction in the H_2/N_2 permeation ratio.

Phenol-Formaldehyde Resin: The phenolic resin coatings were found to decrease the permeation rate by almost an order of magnitude at high loadings; however, the hydrogen-to-nitrogen permeation ratio did not change significantly indicating no significant change in the membrane pore size distribution.

Table 3-3. Permeability of Various Coated Tubes for Different Gases at 20 °C ($K = cm^3/s \cdot cm^2 \cdot mm\ Hg \times 10^3$)

Carbon tube sample	H_2	N_2	He	CO_2	CO
1-μm blank uncoated tube	15.81	7.10	8.33	7.66	7.06
1-μm tube coated 5 times with 10% PAN solution	1.67	0.67	0.89		
0.2-μm blank uncoated tube	6.73	2.62	3.90	2.57	2.55
0.2-μm tube coated 5 times with 1.25% PAN solution	21.21	9.77			
0.2-μm tube coated 5 times with 2.5% PAN solution	23.20	9.81			
0.2-μm tube coated 5 times with 5% PAN solution	11.04	4.97	5.93		
0.2-μm tube coated with 5% PAN solution	11.64	4.97	5.73	5.09	4.99
0.2-μm tube coated with 10% PAN-rapid pyrolysis	5.33	2.18	2.95	2.14	2.18
0.2-μm tube coated with 10% PAN-slow pyrolysis	2.88	1.12			
0.2-μm tube coated 5 times with 10% PFA solution	3.94	1.55			
0.2-μm tube coated with 20% PFA solution	3.55	1.48	2.06	1.49	1.46
0.2-μm tube coated with 40% PFA solution	2.32	0.97	1.45	0.95	0.98
0.2-μm tube coated with 20% phenolic resin, low loading	1.18	0.46			
0.2-μm tube coated with 20% phenolic resin, high loading	0.61	0.24			
0.2-μm tube coated with cellulose	1.67	0.65			
0.2-μm tube coated with FAP resin	0.78	0.32			
0.2-μm coated twice with 10% PAN solution	1.40	0.51			
0.2-μm tube coated with PAN by plasma process	10.56	4.06			
0.2-μm tube coated with FAP resin - Sample A	0.38	0.15			
0.2-μm tube coated with FAP resin - Sample B	0.31	0.11			
0.2-μm tube coated with FAP resin - Sample C	0.82	0.023	0.056	0.018	0.028
0.2-μm tube coated with FAP resin - Sample D	0.08	0.029			
0.2-μm tube coated by carbon from propylene pyrolysis	0.162	0.073			
0.2-μm tube coated with PAN by plasma process - Sample B	5.37	0.12			
0.2-μm tube coated with FAP resin - Sample E	0.33	0.12			
0.2-μm tube coated with FAP resin - Sample F-1	0.013				
0.2-μm tube coated with FAP resin - Sample F-2	0.191	0.073			
0.2-μm tube coated with FAP resin - Sample G-1	0.152	0.054	0.099	0.046	0.052
0.2-μm tube coated with FAP resin - Sample G-2	0.083	0.023		0.019	
0.2-μm tube coated with FAP resin - Sample H	0.041	0.011	0.027	0.0067	

Table 3-4. H_2/N_2 Permeability Ratio ($K_{Hydrogen}/K_{Nitrogen}$) for Various Coated Tubes at 20 °C

Carbon tube sample	H_2/N_2 permeability ratio
1.0-μm blank uncoated tube	2.23
1.0-μm tube coated 5 times with 10% PAN solution	2.50
0.2-μm blank uncoated tube	2.57
0.2-μm tube coated 5 times with 1.25% PAN solution	2.17
0.2-μm tube coated 5 times with 2.5% PAN solution	2.37
0.2-μm tube coated 5 times with 5% PAN solution	2.34
0.2-μm tube coated with 5% PAN	2.34
0.2-μm tube coated with 10% PAN-rapid pyrolysis	2.44
0.2-μm tube coated with 10% PAN-slow pyrolysis	2.58
0.2-μm tube coated 5 times with 10% PFA solution	2.54
0.2-μm tube coated with 20% PFA	2.41
0.2-μm tube coated with 40% PFA	2.40
0.2-μm tube coated with 20% phenolic resin - low loading	2.58
0.2-μm tube coated with 20% phenolic resin - high loading	2.52
0.2-μm tube coated with cellulose	2.56
0.2-μm tube coated with FAP resin	2.47
0.2-μm tube coated twice with 10% PAN solution	2.74
0.2-μm tube coated with PAN by plasma process	2.60
0.2-μm tube coated with FAP resin - Sample A	2.57
0.2-μm tube coated with FAP resin - Sample B	2.77
0.2-μm tube coated with FAP resin - Sample C	3.57
0.2-μm tube coated with FAP resin - Sample D	2.76
0.2-μm tube coated by carbon from propylene pyrolysis	2.22
0.2-μm tube coated with PAN by plasma process - Sample B	2.60
0.2-μm tube coated with FAP resin - Sample E	2.71
0.2-μm tube coated with FAP resin - Sample F-1	
0.2-μm tube coated with FAP resin - Sample F-2	2.61
0.2-μm tube coated with FAP resin - Sample G-1	2.81
0.2-μm tube coated with FAP resin - Sample G-2	3.61
0.2-μm tube coated with FAP resin - Sample H	3.8

Cellulose: Membrane samples prepared with cellulose coating appeared very flaky; therefore, several coatings were applied. Again, a reduction in permeation rate was observed without significant change in the hydrogen-to-nitrogen permeation ratio.

Propylene: Membrane samples modified by propylene pyrolysis indicated more than an order-of-magnitude reduction in permeation rates. However, the hydrogen-to-nitrogen permeation ratios were also reduced significantly indicating a broadening of pore size distribution.

FAP Resin: Pure component permeation studies with membrane samples prepared using this precursor indicated up to two orders-of-magnitude reduction in the permeation rates and significant increase in the ratio of hydrogen-to-nitrogen permeabilities. With some samples, the permeation ratios were found to be close to that expected for a Knudsen diffusion-dominated process. The different samples A through H were prepared with variations in coating and pyrolysis procedures. Because of the promising results obtained with these initial FAP resin samples, further membrane preparation efforts were concentrated on this polymeric precursor. Numerous samples were then prepared with this resin precursor to optimize the coating and pyrolysis process. The variations included coating of polymer by hand versus pressurized coating, number of coatings, sequence of coatings, and pyrolysis temperature. In general, pressurized coatings and lower temperature pyrolysis produced better results; however, the sequence of steps was found to be very important. The permeation results for these samples are shown in Tables 3-5 and 3-6. As the tables indicate, the pure component permeation rates for various samples were found to be inversely proportional to the square root of the molecular weight as shown in Figure 3-8, indicating the presence of a predominantly diffusive flow. As this figure indicates, the hydrogen permeability of these membrane samples ranged from 1×10^{-5} to 5×10^{-5} std $cm^3/(s \cdot cm^2 \cdot mm)$ Hg.

As discussed earlier, of all analysis techniques, permeation measurements provide a direct measure of the effectiveness of the membrane modification process. All other techniques based on BET surface area analysis, mercury porosimeter, and SEM analysis can at best provide a qualitative estimate. BET surface areas measured for selected samples are shown in Table 3-7, which indicates almost no correlation with the observed permeation data shown in Figure 3-8. The pore size distribution for sample K-5 measured with a mercury porosimeter is shown in Figure 3-9, which indicates significant reduction in large pores from that seen in Figure 3-3. Other coated membrane samples also showed pore size distributions similar to that shown in Figure 3-9. SEM analysis of FAP resin-coated samples indicated a nonporous layer of pyrolyzed resin (i.e., no pores above 100 Å, which is the typical resolution of the SEM). However, the SEM plan views also indicated macrocracks in the coated layer, which may be contributing to the viscous flow. An example of the cross section of the coated layer and a plan view of the coating are shown in Figures 3-10 and 3-11, respectively.

Following the tests with the 2-1/2-in. long membrane samples, several 8-in. long membrane samples were prepared with this precursor to conduct mixed gas permeation tests at ambient conditions as well as at HTHP conditions. The HTHP facility developed for these tests and for conducting WGS reaction experiments is described in Section 4.

Table 3-5. Permeability of FAP Resin-Coated Membrane Tube Samples for Different Gases (K = $cm^3/s \cdot cm^2 \cdot mm\ Hg \times 10^3$ at 20 °C)

Carbon membrane tube sample	H_2	N_2	He	CO	CO_2
0.2-μm commercial tube	6.73	2.62	3.90	2.57	2.55
Sample C	0.082	0.023	0.056	0.028	0.018
Sample H	0.041	0.011	0.027		0.0067
Sample K-1	0.0454	0.0141	0.029	0.0149	0.0116
Sample K-2	0.0345	0.0111	0.0244	0.0105	0.0094
Sample K-3	0.112	0.036	0.0738	0.0361	0.0337
Sample K-4	0.0175	0.0049	0.0118	0.0052	0.0037
Sample K-5	0.0114	0.0035	0.0080	0.0031	0.0024
Sample K-6	0.0226	0.0073	0.0151	0.0072	0.0061
Sample K-7	0.0408	0.0137	0.0283	0.0129	0.096
Sample K-8	0.46	0.17			
Sample K-9	0.121	0.0407	0.0759	0.0412	0.0337
Sample K-10	0.541	0.205			
Sample K-11	0.736	0.276			
Sample K-12	0.120	0.0405	0.0785	0.0408	0.0384
Sample K-13	0.629	0.245			
Sample K-14	0.0342	0.0105	0.0227	0.0101	0.0088
Sample K-15	0.0393	0.0120	0.0259	0.0127	0.0094
Sample K-15	0.0927	0.0314	0.0607	0.032	0.0284
Sample K-16	0.033	0.0104	0.0206	0.0101	0.0075
Sample K-17	0.024	0.0083	0.0178	0.0083	0.0063
Sample K-19	0.0392	0.0120	0.0267	0.0125	0.0098
Sample K-20	0.0195	0.0064	0.0139	0.0058	0.0048
Sample K-21	0.0478	0.0169	0.0347		0.0140
Sample K-22	0.0434	0.0152	0.0298	0.0148	0.0125
L-1	0.119	0.0350	0.0792		0.0291
L-2	0.108	0.0354			

Table 3-6. H_2/N_2 Permeability Ratio of Furan Resin-Coated Samples ($K_{Hydrogen}/K_{Nitrogen}$ at 20 °C)

Carbon membrane tube sample	H_2/N_2 permeability ratio	Carbon membrane tube sample	H_2/N_2 permeability ratio
0.2-μm commercial tube	2.57	Sample K-12	2.96
Sample C	3.57	Sample K-13	2.56
Sample H	3.8	Sample K-14	3.26
Sample K-1	3.22	Sample K-15	3.28
Sample K-2	3.10	Sample K-15	2.96
Sample K-3	3.11	Sample K-16	3.09
Sample K-4	3.58	Sample K-17	2.89
Sample K-5	3.20	Sample K-19	3.27
Sample K-6	3.09	Sample K-20	3.02
Sample K-7	3.38	Sample K-21	2.85
Sample K-8	2.67	Sample K-22	2.85
Sample K-9	2.97	L-1	3.40
Sample K-10	2.65	L-2	3.05
Sample K-11	2.57		

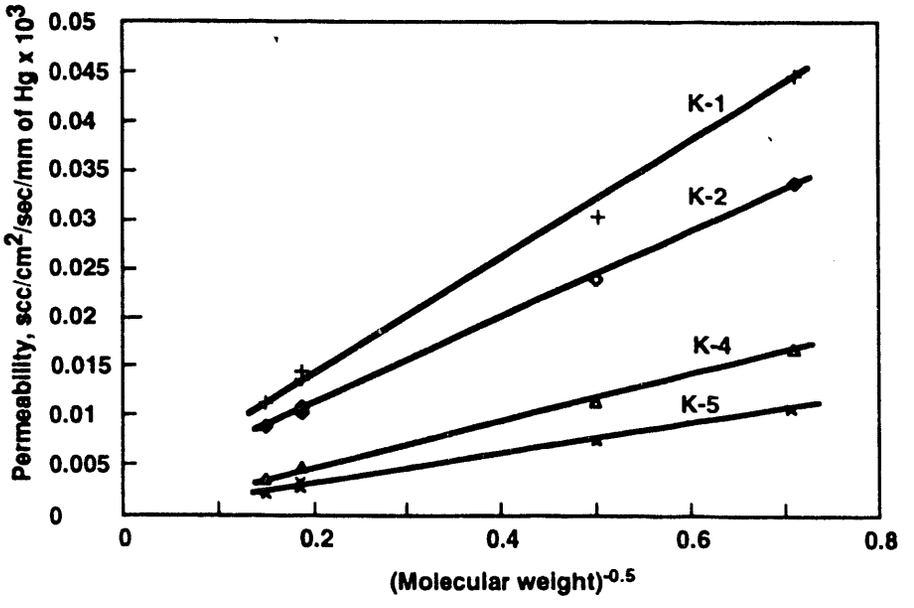

Figure 3-8. Pure component permeabilities for various FAP resin-coated samples.

Table 3-7. BET Surface Area of Selected FAP Resin-Coated Samples

Membrane sample	BET surface area (m^2/g)
Blank (0.2 μm)	10.3
K-1	17.8
K-3	29.0
K-4	24.1
K-5	14.6
K-6	24.8
K-10	20.5

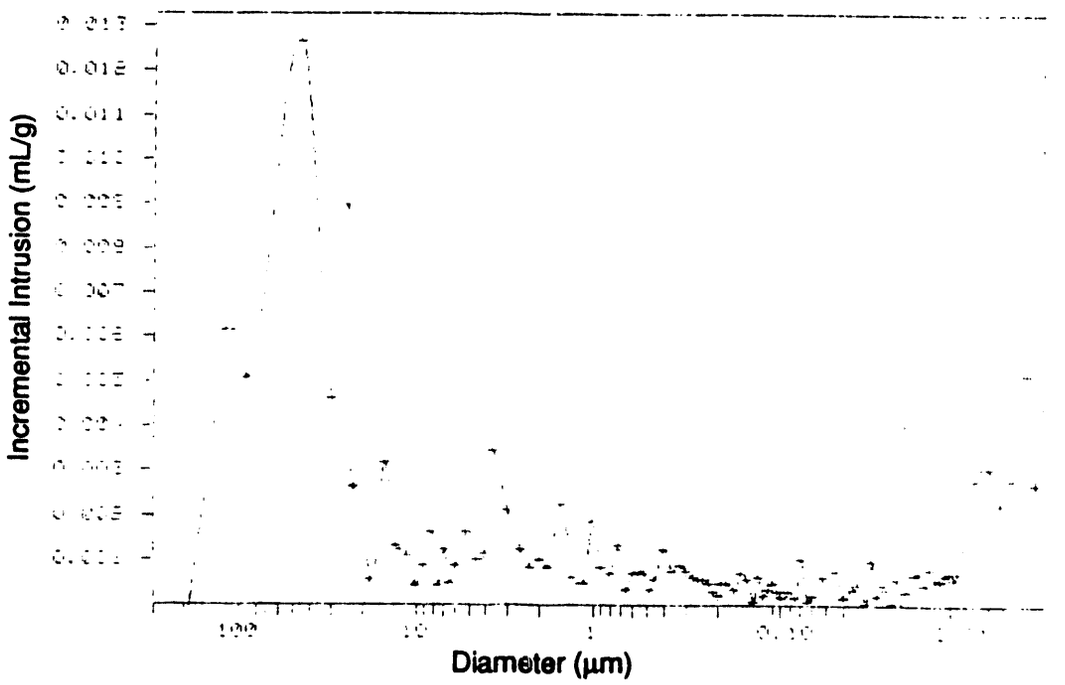

Figure 3-9. Pore size distribution for FAP resin-coated sample, K-5.

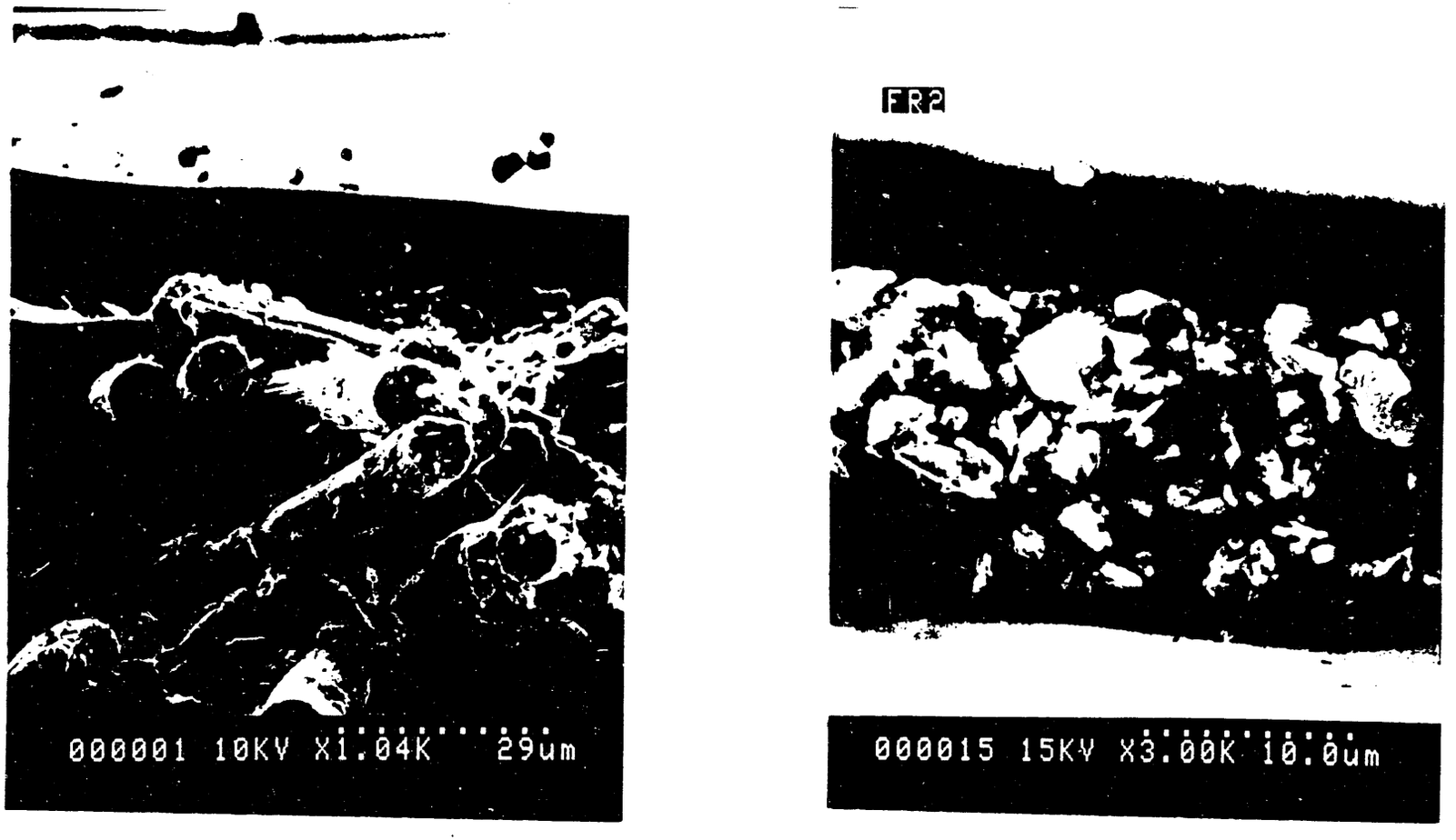

Figure 3-10. Typical cross section of a pyrolyzed FAP resin coating layer.

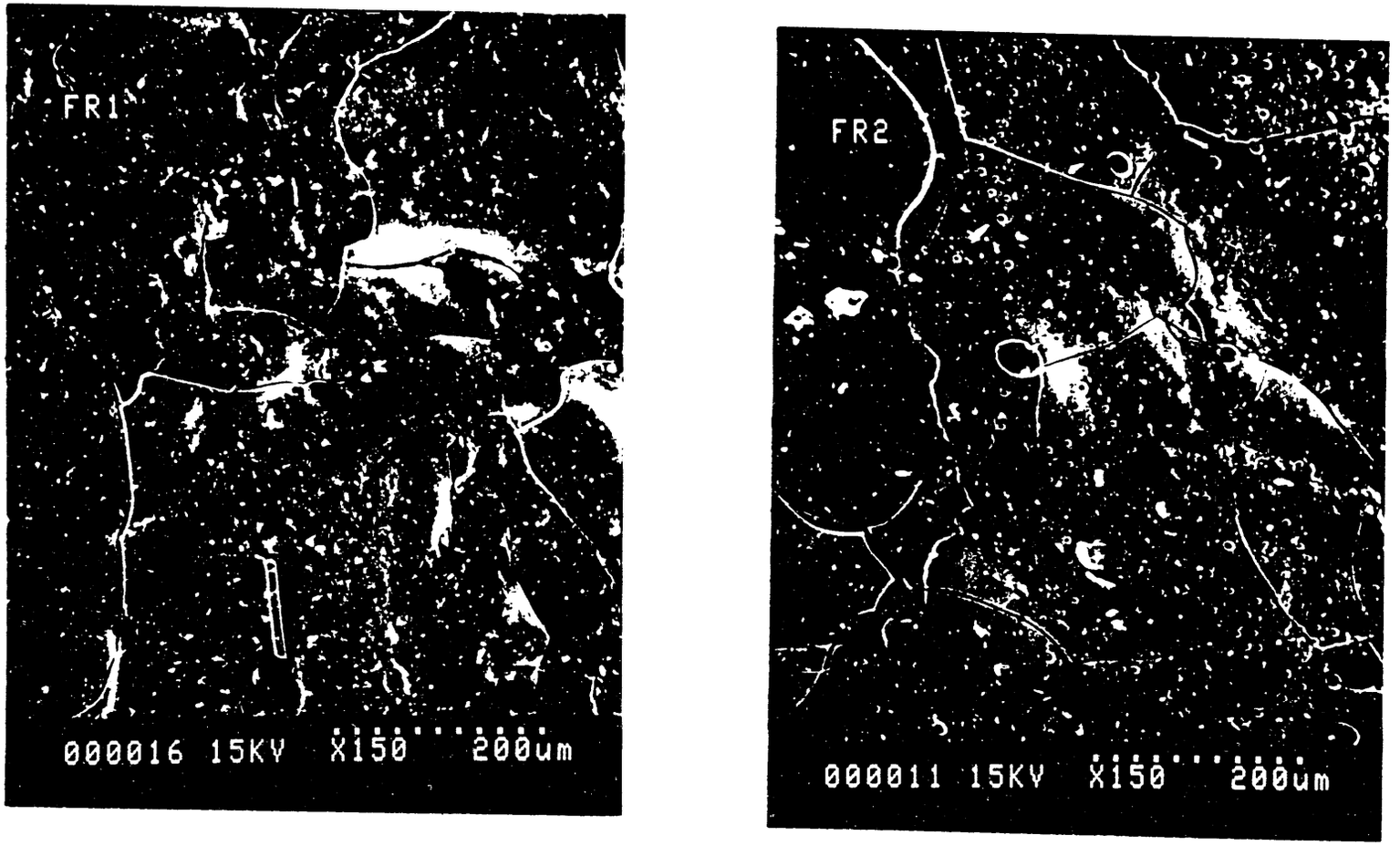

Figure 3-11. Typical plan view of a pyrolyzed FAP resin coating layer.

SECTION 4

HTHP TESTING OF CARBON MEMBRANES

The membranes prepared according to the procedures discussed in Section 3 were tested in the HTHP environment to evaluate the potential for separation of hydrogen by Knudsen diffusion, to measure the extent of WGS, and to determine the effect of various parameters on the extent of the shift reaction and hydrogen separation. The overall objective of these tests was to determine the increase in hydrogen yield in the shift reaction due to simultaneous separation of the product hydrogen. The parameters of interest were gas flow rate (residence time), gas composition, H_2O:CO molar ratio, gas temperature and pressure, transmembrane pressure drop, and sweep gas flow rate. Preliminary HTHP studies indicated no significant WGS reaction with the catalyst impregnated in the pores of carbon membrane tubes. With membrane tubes packed with 1/8-in. catalyst pellets, WGS reaction was observed with only a small effect of residence time on CO conversion presumably due to a small catalyst bed. Therefore, all of the HTHP testing was conducted with membrane tubes packed with catalyst pellets (instead of membrane tubes with catalyst impregnation in pores) in order to ensure substantial CO conversion during these experimental runs.

4.1 HTHP Test Facility

For HTHP testing of carbon membranes a test facility was constructed as shown schematically in Figure 4-1. The gas delivery system can supply the coal gas composition to be used as well as the inert sweep gas. This system also has the capability to provide the required gases for catalyst calcination/activation. The flow rate of the gases is controlled by mass flow controllers. The water vapor required for the WGS reaction testing is generated by a high-pressure positive displacement pump and a water heater. The water vapor is mixed with a preheated test gas mixture stream and is introduced inside the membrane tube while the sweep gas stream flows countercurrently on the outside of the tube. The membrane tube is housed inside a stainless steel jacket reactor and the reactor system is maintained at a controlled temperature using a two-zone furnace. The outer 1-1/2-in. I.D. stainless steel jacket is designed to withstand up to 400 psia pressure and 700 °C temperature. The 8-mm O.D. membrane tube is connected to 1/4-in. stainless-steel tubing using appropriate fitting and graphite seals. The exit test gas and sweep gas streams are cooled to remove the unreacted water vapor before they exit through dryers, filters, and back pressure regulators (BPRs). The BPRs control the individual stream pressures to provide the desired transmembrane pressure drops, as monitored by a differential pressure gauge. The transmembrane pressures can be controlled from 0.02 psia to 100 psia. The sweep gas and test gas streams are analyzed by an outline gas chromatograph (GC). Test gas flow on the order of 1 std L/min (slpm) can provide about 2 to 3 seconds of membrane tube residence time in this system at 300 psi pressure.

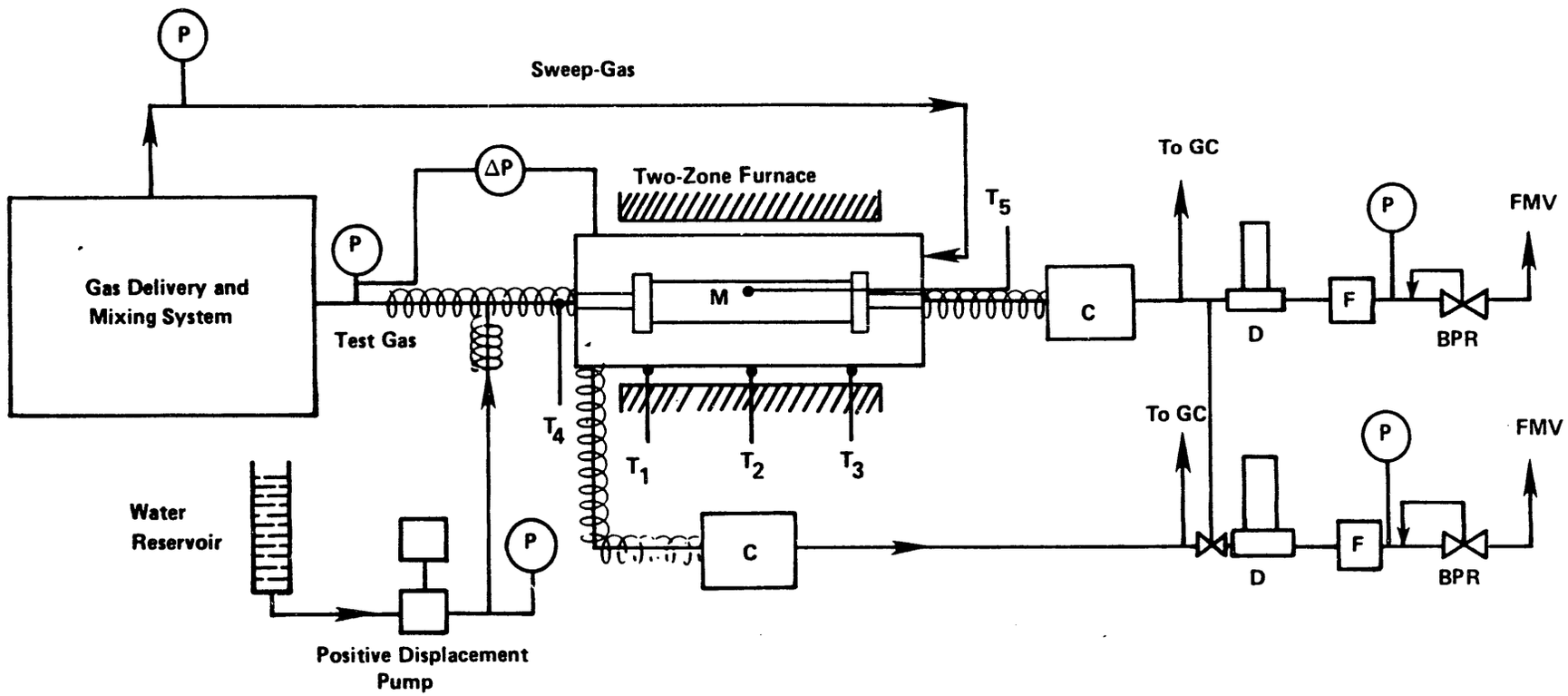

FMV:	Flow Meter and Vent
M:	Tubular Membrane Module
P:	Pressure Gauge
ΔP:	Differential Pressure Gauge
T_1-T_6:	Temperature Measurement and Control
D:	High Pressure Drier
BPR:	Back Pressure Regulator
F:	Filter

	Preheater/Heated Lines
GC:	Gas Chromatograph
C:	Condensation and Liquid Separation System

Figure 4-1. Schematic of an HTHP membrane test facility.

4.2 Equilibrium Reactor

The modified carbon membrane tubes are microporous and are expected to separate hydrogen from other heavier gases by Knudsen diffusion mechanism. This mechanism provides only a relative separation of gases based on their differing permeation rates. The flux rate of a gas species through such a membrane is inversely proportional to the square root of its molecular weight and is directly proportional to its partial pressure difference across the membrane. To reduce the permeation of reactants before reaction, it is advantageous to delay the membrane separation until after the reacting gas mixture has reached a near-equilibrium composition. This minimizes the partial pressure of the reactants, i.e., CO and H_2O, and thereby reduces their loss through permeation. The equilibrium constant, K_{eq}, depends on the membrane reactor temperature and is given by (Singh and Saraf, 1977)

$$K_{eq} = EXP\left[\left(\frac{4.187x10^7}{T} - 4.277x10^4 + 11.502T - 1.897x10^{-3}T^2 - 841.75\ lnT\right)/R\right] \quad (4\text{-}1)$$

where

T = reaction temperature in K
R = gas constant 8314 (N·m/kmol K).

To achieve the near-equilibrium composition at the reaction conditions prior to membrane separation, the test gas and water vapor mixture was passed through a 1/2-in. diameter and 4-in. long tubular "equilibrium" reactor packed with 1/8-in. WGS catalyst pellets and maintained at the same temperature as the membrane reactor. The observed composition exiting the equilibrium reactor indicated a close approach to the equilibrium constant predicted by Equation (4-1). The near-equilibrium gases entered the membrane reactor, also packed with catalyst pellets, to allow hydrogen separation and further CO conversion by shifting the equilibrium toward hydrogen.

4.3 Sealing Carbon Membrane Tubes

Sealing the carbon membrane tubes/metal fitting connection is essential to provide accurate permeation data. The problem is especially severe at HTHP conditions of the reactor and the problem is further magnified for those membranes with very low permeation rates of the gases. Custom-made 8-mm graphite ferrules were used in the carbon tube to stainless steel tube joints. The ends of the carbon tube were first polished and then sealed with a high-temperature sealant to provide a smooth surface. The carbon tube was then connected to metal tubing using 8-mm to 1/4-in. Swagelock fitting. The graphite ferrules were found to provide an adequate seal up to the 200-psig feed gas pressure used during the HTHP experiments.

4.4 Mixed Gas Permeation Studies

The HTHP facility was first used to conduct mixed gas separation studies both at ambient conditions and at high-temperature conditions using the 8-in. long membrane tube samples prepared with FAP resin. Different test gas compositions consisting of CO, CO_2, H_2, and N_2 and typical of coal gas were used for these tests. The test gas was fed inside the tubular membrane. The feed gas flow rate was controlled by a mass flow controller and its pressure was controlled by a BPR. Pure N_2 was used as a sweep gas, which was fed countercurrently on the outside of the membrane tube. The flow rate and the pressure of the sweep gas were also controlled. For a given steady-state flow and given pressure conditions, the exit sweep and test gases were sampled using an on-line GC sequentially. About 30 minutes was allowed after any change in flow or pressure conditions to attain a steady state. The permeate rate was usually kept small enough so that the test gas composition was held approximately constant. The sweep gas composition measured at different transmembrane pressure drops thus allowed determination of gas separation factors as a function of transmembrane pressure drop. The high-temperature permeation studies were typically conducted at temperatures up to 425 °C. For some membranes sample permeation studies were also conducted at intermediate temperatures of 100 and 200 °C.

Table 4-1 provides the gas separation factors observed with different membrane samples prepared with slight variations in the preparation procedure. The table provides separation factors for both H_2/CO and H_2/CO_2 separation (i.e., K_{H_2}/K_{CO} and K_{H_2}/K_{CO_2}) as a function of temperature and transmembrane pressure drops. All of the separation factor data indicate strong dependence on the gas temperature as well as gas pressure as shown in typical results presented in Figures 4-2, 4-3, and 4-4. The observed separation factors for the modified membranes are significantly higher than those for unmodified blank membranes, indicating significant reduction in membrane pore size. However, these separation factors are lower than the theoretical maximum values of 3.7 and 4.7 for H_2/CO and H_2/CO_2 separations, respectively, indicating significant viscous flow along with Knudsen diffusion flow.

The overall permeation flux for component i through these membranes, N_i, may be described as

$$N_i = \underbrace{\frac{\phi D_i \Delta P_i}{\tau RTl}}_{\textit{diffusive flow}} + \underbrace{\frac{\phi r^2 P \Delta P X_i}{8 \tau \mu_m RTl}}_{\textit{viscous flow}} \qquad (4\text{-}2)$$

where

ϕ	= porosity	T	= temperature, K
D_i	= diffusion coefficient, m^2/s	ι	= membrane thickness, m
ΔP_i	= partial pressure difference for component i, Pa	r	= membrane pore radius, m
		P	= feed side gas pressure, Pa
τ	= tortuosity factor	X_i	= feed side mol fraction of component i
R	= gas constant, N·m/KmolK	μ_m	= gas mixture viscosity, kg/m·s.

Table 4-1. H_2/CO and H_2/CO_2 Separation Factors in Mixed Gas Permeation Tests (Sweep Side Pressure ~5 psig)

Sample	Temperature, °C	H_2/CO separation factors transmembrane pressure drop, psi					H_2/CO_2 separation factors transmembrane pressure drop, psi				
		2	5	10	20	40	2	5	10	20	40
Blank	400	1.85	1.35	1.27	-	-	2.03	1.40	1.33	-	-
L-2	25	2.16	1.85	1.48	1.34	-	3.35	2.09	1.59	1.35	-
	100	-	2.31	1.94	-	-	-	2.58	2.01	-	-
L-3	20	-	1.50	1.32	-	-	-	1.58	1.34	-	-
	400	-	2.69	2.26	1.92	1.52	-	3.26	2.63	2.06	1.66
L-4	20	2.01	1.36	1.16	1.13	1.05	1.99	1.43	1.21	1.13	1.07
L-5	20	1.89	1.24	1.21	1.15	1.07	2.17	1.31	1.27	1.19	1.09
	400	3.13	2.43	2.05	1.62	1.35	3.55	2.77	2.21	1.71	1.46
L-6	400	2.05	1.75	1.45	1.26	1.14	2.29	1.83	1.51	1.3	1.17
L-6'	25	-	1.94	1.64	-	-	-	2.05	1.62	-	-
	100	-	2.39	1.92	-	-	-	2.65	1.99	-	-
	200	-	2.69	2.13	-	-	-	2.98	2.27	-	-
	400	3.25	2.58	2.33	1.94	1.56	4.07	3.17	2.72	2.11	1.66
L-7	25	1.61	1.2	1.19	1.13	-	1.73	1.24	1.21	1.13	-
	200	2.49	1.62	1.37	-	-	2.84	1.71	1.40	-	-
	400	2.97	2.11	1.61	1.39	1.23	3.38	2.34	1.74	1.46	1.26
L-7'	25	2.45	1.76	1.39	--	--	3.43	1.88	1.45	--	--
	425	2.96	2.68	2.30	1.86	1.54	4.38	3.58	2.86	2.17	1.7

(continued)

Table 4-1 (continued)

Sample	Temperature, °C	H_2/CO separation factors transmembrane pressure drop, psi					H_2/CO_2 separation factors transmembrane pressure drop, psi				
		2	5	10	20	40	2	5	10	20	40
L-9	25	1.53	1.09	1.05	-	-	1.61	1.12	1.06	-	-
	200	2.36	1.49	1.23	-	-	2.68	1.55	1.26	-	-
	400	2.75	1.69	1.38	-	-	3.38	1.84	1.45	-	-
L-10	23	2.94	2.0	1.81	1.34	1.21	3.18	2.24	1.67	1.37	1.23
	400	-	3.16	2.53	1.93	1.56	3.66	2.84	2.39	1.92	1.61
L-11	24	1.82	1.49	1.28	1.13	1.0	2.01	1.47	1.26	1.13	1.0
	400	2.59	1.82	1.6	1.32	1.14	3.04	2.1	1.68	1.39	1.21
L-11'	25	2.28	1.88	1.55	1.28	1.20	2.80	2.09	1.63	1.34	1.21
	425	2.51	2.16	1.88	1.58	1.41	3.68	2.78	2.25	1.80	1.53
L-12	23	2.61	2.06	1.62	1.36	1.19	2.46	2.03	1.57	1.33	1.16
	425	2.94	2.85	2.78	2.53	2.08	4.28	3.95	3.53	2.92	2.30
L-13	24	2.5	2.05	1.64	1.39	1.26	2.79	2.21	1.80	1.48	1.27
	425	3.73	2.62	2.32	2.05	1.85	3.82	3.31	2.97	2.41	1.93
L-14	25	2.27	1.70	1.39	1.18	1.13	3.04	2.16	1.6	1.28	1.17
	425	1.92	1.85	1.69	1.48	1.30	3.21	2.70	2.20	1.73	1.42
L-15	24	2.63	2.1	1.62	1.37	1.22	2.64	2.1	1.59	1.35	1.21
	425	3.47	2.86	2.46	2.13	1.67	4.03	3.59	2.97	2.39	1.87
L-16	22	2.39	1.71	1.35	1.24	1.13	2.59	1.72	1.35	1.23	1.12
	425	3.25	2.66	2.31	1.86	1.49	3.82	3.09	2.63	2.06	1.60
L-17	23	2.74	1.98	1.56	1.34	1.21	3.21	2.05	1.59	1.35	1.22
	425	3.42	3.08	2.69	2.25	1.76	4.01	3.61	3.11	2.55	2.01

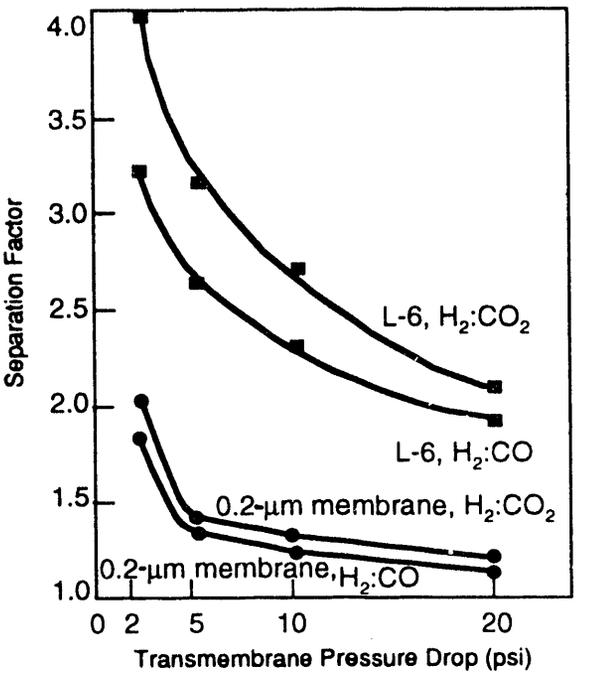

Figure 4-2. Observed gas separation factors at 400 °C for an unmodified membrane and membrane sample L-6.

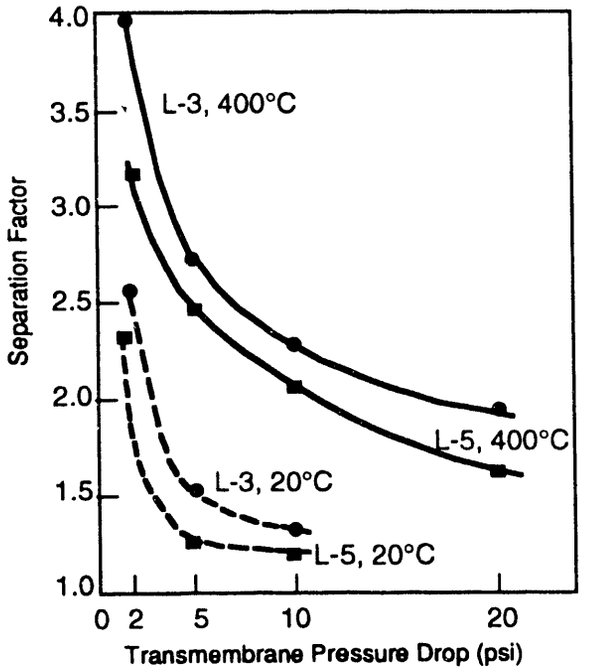

Figure 4-3. Effect of temperature and transmembrane pressure drop on H_2/CO separation factor.

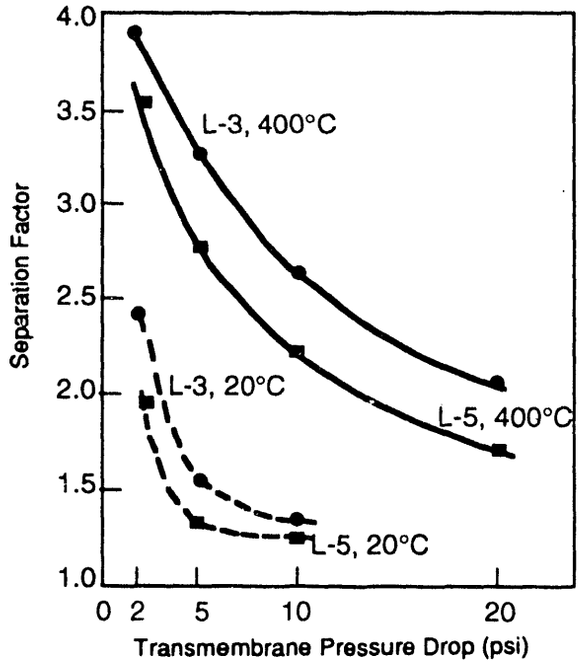

Figure 4-4. Effect of temperature and transmembrane pressure drop on H_2/CO_2 separation factor

Viscous flow is directly proportional to the gas pressure and inversely proportional to the gas viscosity. Both the gas viscosity and the Knudsen diffusion coefficient increase with gas temperature. Higher gas temperature and lower feed gas pressure thus increase the separation factors as expected by decreasing the viscous flow contribution and increasing the diffusive flow. For high-pressure commercial application of these membranes the viscous flow contribution must be reduced further by additionally decreasing the membrane pore size. The hydrogen flux rates also need to be increased by decreasing the effective membrane thickness.

In Equation (4-2), the partial pressure difference for component i, ΔP_i may be approximated by $P \cdot x_i$. This assumption is valid for large transmembrane pressure drops, or for very low permeate concentrations in the sweep gas. In the HTHP experiments, the permeate concentrations in the sweep nitrogen gas were quite low because of low permeation rates across the membrane. With this assumption, Equation (4-2) may be simplified to express the component fluxes as a function of total pressure drop and the feed side component mol fraction:

$$N_i = (A_i + B\ \Delta P)\ x_i\ . \qquad (4\text{-}3)$$

The coefficient A_i incorporates the component diffusivity D_i, which is inversely proportional to the square root of the component molecular weight M_i. A separation factor between two components (i.e., the ratio of component permeabilities) is given by

$$\alpha_{12} = \frac{K_1}{K_2} = \frac{N_1/x_1}{N_2/x_2} . \tag{4-4}$$

Substituting Equation (4-3)

$$\alpha_{12} = \frac{A_1 + B\Delta P}{A_2 + B\Delta P} = \frac{A_1 + B\Delta P}{A_1\sqrt{\frac{M_1}{M_2}} + B\Delta P} . \tag{4-5}$$

Rearranging Equation (4-5), the separation factor α_{12} may be directly related to the transmembrane pressure drop, ΔP:

$$\frac{\alpha_{12}}{\alpha_{12} - 1}\left(1 - \sqrt{\frac{M_1}{M_2}}\right) = 1 + \frac{B}{A_1}\Delta P . \tag{4-6}$$

Equation (4-6) predicts a straight line when the left side of Equation (4-6) is plotted against ΔP. This relationship is verified by the experimental mixed-gas permeation data for membrane samples L-3 and L-5 as shown in Figure 4-5. The slope of the lines in this figure indicates the relative contribution of the viscous and diffusive flow. A horizontal line flush with the x-axis would indicate a completely diffusion-controlled process with no viscous contributions. As seen from Figure 4-4, both the membrane samples L-3 and L-5 indicated significant viscous flow contribution.

4.5 WGS Reaction Studies

A number of WGS reaction studies were conducted using some of the long (8-in.) membrane tube samples. A feed gas composition typical of Manufacturing and Technology Conversion International, Inc. (MTCI) gasifier gas was used as the test gas consisting of 49.7 percent H_2, 13.4 percent CO, 23.5 percent CO_2, 12 percent N_2, and 1.4 percent H_2S. Water was added separately to the dry gas to provide a desired H_2O:CO mol ratio.

4.5.1 Membrane Testing Procedure

The test gas was preheated using heating tapes, and water vapor was injected into it to generate a desired steam concentration. A known amount of water vapor was generated by injecting accurately metered amounts of water using a high-pressure high-performance liquid

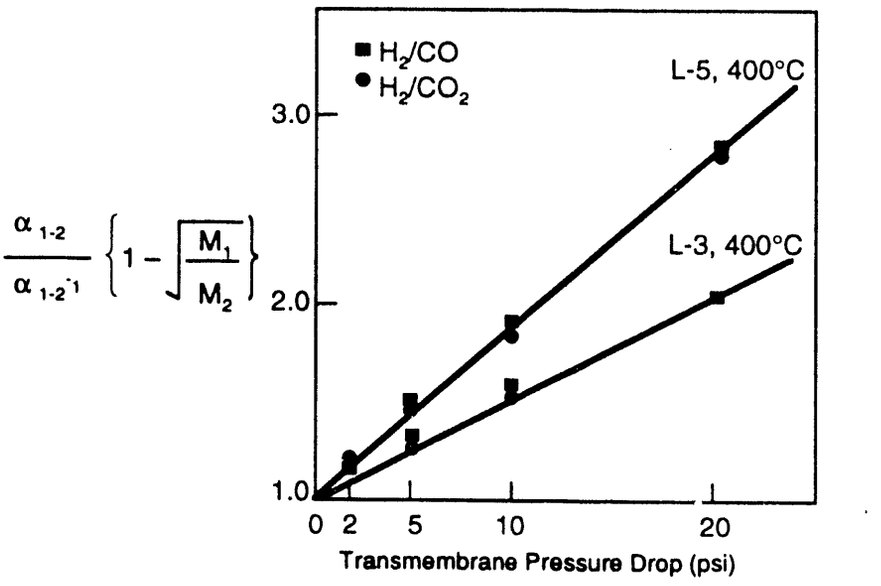

Figure 4-5. Observed H_2/CO and H_2/CO_2 separation factor relationship with ΔP.

chromatography (HPLC) syringe pump. The gas mixture was then passed through heat-traced lines first into the equilibrium reactor and subsequently into the membrane reactor module. The membrane module was heated using a two-zone furnace capable of attaining temperatures up to 1,000 °C. The two-zone furnace has a heated length of 12 in. and was placed vertically with the flow of test gas downwards. The test membrane module has an outer stainless steel jacket capable of withstanding the pressure and temperature conditions of the testing (300 psig and 450 °C). The nitrogen sweep gas flowed through the outer jacket countercurrently to the test gas flow.

The test gas was passed through the membrane module and then sent to a condensation system consisting of a steam condenser and catchpot. After leaving the catchpot, the test gas was dried and filtered at high pressure and then vented through a BPR that controlled the test gas side pressure. The sweep gas, along with the gases permeated into it, were also sent through a condensation system and then vented through another BPR. The two BPRs control the gas pressures on each side of the membrane and thus control the transmembrane pressure drop, which is an important operating parameter. The transmembrane pressure drop was monitored by a differential pressure gauge with pressure leads in the respective gas streams. Samples from the test gas and the sweep gas were sequentially analyzed using a GC. All the bulk gases (H_2, CO, N_2, CO_2) and H_2S were analyzed to determine the composition of the test and sweep gas streams. Calibration gases were run through the GC prior to an experimental run to obtain appropriate calibration factors.

The test and sweep gas flow rates and reactor conditions of temperature, pressure, and transmembrane pressure drop were held constant until steady-state gas concentrations were observed in sequential GC analyses. The outlet gas stream compositions and the known input gas flow rates and compositions enabled determination of the extent of WGS reaction as well as permeation rates of all gases. The relative permeation rates also determined the respective separation factors. All gases except N_2 permeated from test gas side to sweep gas side, whereas nitrogen permeated from sweep gas side to test gas side due to its greater partial pressure on the sweep side. Hydrogen permeation increased by increasing the transmembrane pressure drop. Thus, the effect of membrane separation on CO conversion was determined by comparing the observed CO conversions for different transmembrane pressure drops.

4.5.2 WGS Catalyst

A commercial WGS catalyst was used to pack both the equilibrium reactor and the membrane reactor. The catalyst used was in the form of 1/8-in. extrusion pellets with a surface area of about 150 m^2/g. This catalyst consisted of about 12 percent MoO_3 and 3.2 percent CoO in an alumina base and was expected to be active in a 290 to 455 °C range. These oxide pellets were sulfided by passing 1 percent H_2S in an H_2/N_2 mixture over the catalyst pellets at 400 °C for 16 hours. The sulfided catalyst pellets were stable in the presence of the H_2S in the test gas and were found to provide significant WGS catalytic activity in the HTHP studies.

4.5.3 HTHP Test Parameters

Several important parameters and their ranges during these experiments are as follows:

- **Carbon Membranes**: Six carbon membrane tubes (L-6, L-12, L-13, L-15, L-16, L-17) were used in these studies. The tubes were prepared using different coating and pyrolysis conditions.

- **Test Gas Composition**: A test gas composition representing the MTCI char gasifier was used to conduct these tests and consisted of 13.4 percent CO, 49.7 percent H_2, 23.5 percent CO_2, 12.0 percent N_2, and 1.4 percent H_2S on a dry basis. Premixed gas cylinders with the above-mentioned gas composition were obtained to provide the dry test gas mixture.

- **Test Gas Temperature**: The temperature of both the equilibrium reactor and the membrane reactor was kept the same and was approximately 425 °C.

- **Test Gas Pressure**: Feed gas pressures ranged from 10 psig to 200 psig. For most runs, transmembrane pressure drops of 5, 10, 20, and 40 psi were used with a sweep gas side pressure of 5 to 9 psig. A certain minimum sweep gas pressure was needed to maintain adequate flow into the GC sampling system. For membranes L-12 and L-13, WGS experiments were also conducted at high-pressure drops of 50 and 100 psi with the feed pressures of 100, 150, and 200 psig.

- **Test Gas Flow Rate**: Dry test gas flow rates of 250 std cm^3/minute (sccm) and 500 sccm were used.

- **Water-to-CO Molar Ratio**: Water-to-CO molar ratios of 2:1 to 4:1 were used.

- **Sweep Gas Flow Rate**: A sweep gas flow rate of 200 sccm was used in all runs.

4.5.4 WGS Experiment Results

The results obtained with membrane tube samples L-6, L-12, L-13, L-15, L-16, and L-17 are presented in Tables 4-2 through 4-7. The CO conversion is generally seen to increase moderately with an increase in the transmembrane pressure drop or hydrogen permeation rate. The amount of hydrogen permeated in all of the runs represents only a small stage cut because of the low permeation rate through the membrane and the limited surface area that could be used in these experiments. Thus, the noticeable increase in CO conversion even with such a small stage cut of 0.1 or less is encouraging. As discussed in the next model simulation section, a significant stage cut is needed to obtain such a noticeable increase in the CO conversion.

Based upon permeation rates of H_2 and CO_2, H_2/CO_2 separation factors were also determined as shown in these tables. These separation factors compare well with those observed in mixed gas permeation tests. With samples L-12 and L-13, some WGS reaction runs were carried out at high pressure and pressure drops. The H_2/CO_2 separation factors were observed to decrease with increasing system pressure and pressure drop as expected. At feed pressure of 200 psi and pressure drop of 100 psi, an H_2/CO_2 separation factor of only 1.5 was observed compared to a theoretical value of 4.7 for the Knudsen flow regime.

Table 4-2. Effect of H_2 Permeation on CO Conversion: Temperature = 425 °C, Test Gas Flow = 500 sccm, Membrane Sample = L-6 (MTCI Gasifier Gas Composition)

Pressure drop (psi)	H_2 transferred (sccm)	CO conversion (%)		H_2/CO_2 separation factor
		H_2O:CO = 3:1	H_2O:CO = 2.1	
No permeation	--	45.0	23.0	--
5	9.9	48.9	26.0	3.9
10	13.0	53.5	34.3	3.0
20	20.4	57.2	41.9	2.5
40	35.4	60.9	45.9	1.9

Table 4-3. Effect of H_2 Permeation on CO Conversion: Temperature = 425 °C, Nitrogen Sweep Flow = 200 sccm, Membrane Sample = L-12 (MTCI Gasifier Gas Composition)

Feed pressure (psig)	Membrane pressure drop (psia)	Feed flow (sccm)	H_2O:CO mol ratio	CO conversion (%)	Hydrogen transferred (sccm)	H_2/CO_2 separation factor
9	5	500	3:1	44.7	9.0	4.3
14	10	500	3:1	50.0	12.3	3.9
24	20	500	3:1	51.7	17.6	3.2
46	40	500	3:1	58.8	27.4	2.3
100	50	500	3:1	58.4	37.3	1.9
150	50	500	3:1	60.8	39.8	1.7
200	100	500	3:1	59.4	70.9	1.4

Table 4-4. Effect of H_2 Permeation on CO Conversion: Temperature = 425 °C, Nitrogen Sweep Flow = 200 sccm, Membrane Sample = L-13 (MTCI Gasifier Gas Composition)

Feed pressure (psig)	Membrane pressure drop (psia)	Feed flow (sccm)	H_2O:CO mol ratio	CO conversion (%)	Hydrogen transferred (sccm)	H_2/CO_2 separation factor
12	5	500	2:1	43.5	5.1	4.8
17	10	500	2:1	39.2	6.5	4.5
28	20	500	2:1	41.3	9.0	3.5
44	40	500	2:1	40.0	14.1	2.7
46	40	500	1.5:1	29.3	14.8	2.7
46	40	500	3:1	54.9	13.3	2.7
26	20	500	3:1	53.6	8.7	3.4
11	5	500	3:1	50.7	4.8	4.5
10	5	250	4:1	63.1	4.6	4.5
16	10	250	4:1	65.0	5.9	4.0
26	20	250	4:1	66.0	8.2	3.3
43	40	250	4:1	65.2	13.7	2.6
26	20	250	3:1	62.8	8.6	3.3
15	10	250	3:1	56.4	6.3	4.0
10	5	250	3:1	56.0	5.4	4.4
150	50	500	3:1	54.4	21.9	1.9
100	50	500	3:1	50.7	19.5	2.1
200	100	500	3:1	59.2	37.7	1.5

Table 4-5. Effect of H_2 Permeation on CO Conversion: Temperature = 425 °C, Nitrogen Sweep Flow = 200 sccm, Membrane Sample = L-15 (MTCI Gasifier Gas Composition)

Feed pressure (psig)	Membrane pressure drop (psia)	Feed flow (sccm)	H_2O:CO mol ratio	CO conversion (%)	Hydrogen transferred (sccm)	H_2/CO_2 separation factor
14	5	500	3:1	53.0	8.3	3.2
18	10	500	3:1	53.4	10.8	2.6
29	20	500	3:1	53.4	16.9	2.1
49	40	500	3:1	54.6	30.4	1.7
14	5	500	2:1	39.5	9.4	3.2
18	10	500	2:1	39.5	12.6	2.5
29	20	500	2:1	40.4	19.4	2.0
49	40	500	2:1	40.1	35.2	1.6
14	5	250	4:1	67.4	8.4	2.9
18	10	250	4:1	68.3	10.5	2.5
29	20	250	4:1	69.0	17.1	1.9
49	40	250	4:1	70.3	32.9	1.5

Table 4-6. Effect of H_2 Permeation on CO Conversion: Temperature = 425 °C, Nitrogen Sweep Flow = 200 sccm, Membrane Sample = L-16 (MTCI Gasifier Gas Composition)

Feed pressure (psig)	Membrane pressure drop (psia)	Feed flow (sccm)	H_2O:CO mol ratio	CO conversion (%)	Hydrogen transferred (sccm)	H_2/CO_2 separation factor
13	5	500	3:1	52.1	14.4	3.1
18	10	500	3:1	53.3	18.0	2.6
30	20	500	3:1	55.0	29.4	2.0
49	40	500	3:1	54.7	52.2	1.6
14	5	250	4:1	66.4	14.1	2.9
19	10	250	4:1	67.5	19.5	2.3
27	20	250	4:1	68.0	28.8	1.9
50	40	250	4:1	67.8	50.9	1.7

Table 4-7. Effect of H_2 Permeation on CO Conversion: Temperature = 425 °C, Nitrogen Sweep Flow = 200 sccm, Membrane Sample = L-17 (MTCI Gasifier Gas Composition)

Feed pressure (psig)	Membrane pressure drop (psia)	Feed flow (sccm)	H_2O:CO mol ratio	CO conversion (%)	Hydrogen transferred (sccm)	H_2/CO_2 separation factor
10	5	500	3:1	53.6	7.2	3.6
17	10	500	3:1	54.8	9.3	2.9
30	20	500	3:1	55.9	15.7	2.2
50	40	500	3:1	57.2	26.2	1.7

SECTION 5

PROCESS MODELING

To determine the potential of increased CO conversion in WGS reaction due to simultaneous hydrogen separation, a simplified process model was developed. This model takes into account permeation of gases across a membrane based on transmembrane partial pressure differences for each permeating species and its permeability with respect to a reference component. The permeability ratios of different gases are assumed to be constant during membrane separation in this model. The model further assumes that the WGS reaction is not limited by chemical kinetics and thus the feed gas stream is assumed to be continuously at equilibrium throughout the membrane reactor. The reaction is assumed to occur only on the feed side of the membrane due to catalyst loading on the feed side only. The membrane reactor is assumed to be isothermal, thus the equilibrium constant is assumed to be the same throughout the reactor. As the gases permeate through the membrane, the feed side composition changes due to differences in permeation rates of different gases. Thus, the equilibrium compositions change continuously through the membrane reactor. The pressures on both sides of the membrane are further assumed to be constant in the reactor.

Figure 5-1 shows a schematic of a section of a membrane reactor of surface area dA. The pressures on the feed and permeate side are assumed to be P_1 (atm) and P_2 (atm), respectively. Q (mol/s) is molar feed gas flow entering the reactor with y_i mol fraction of component i. R (mol/s) is molar flow of permeate entering the reactor with x_i mol fraction of component i. dQ, dR are molar flow rate changes in the reactor section and dy_i and dx_i are respective mol fraction changes for component i. N_i (mol/s) is the molar flow of component i across the membrane. The feed and permeate flows are shown countercurrent to each other in this schematic; however, rate relations are developed in this section for both the cocurrent and countercurrent flow schemes.

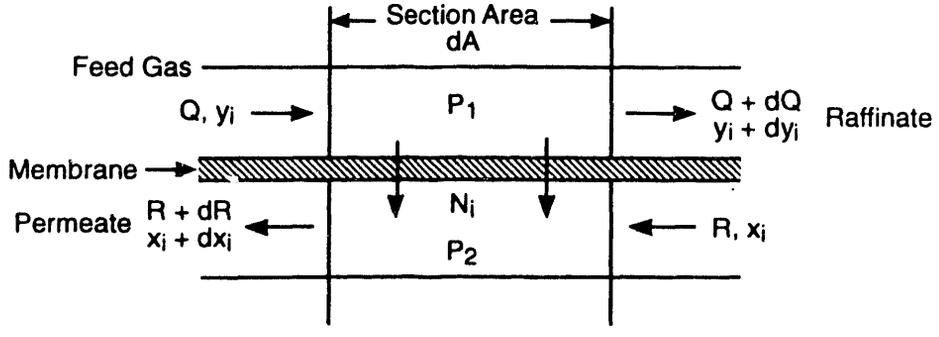

Figure 5-1. Schematic of a membrane reactor system.

The molar flow of component i, N_i, across the membrane is expressed by

$$N_i = (P_1 y_i - P_2 x_i) K_1 \alpha_{i,1} dA \tag{5-1}$$

where, K_1 is the permeability of reference component 1, mol/cm^2-s-atm and, α_{i1} is the permeability ratio of component i with respect to component 1 = K_i/K_1.

Defining a membrane pressure ratio $P_r = P_1/P_2$, the above equation may be rewritten as

$$N_i = (P_r Y_i - x_i) \alpha_{i,1} K_1 P_2 dA \ . \tag{5-2}$$

The changes in total molar flows through the reactor section, dQ and dR, are given by

$$dQ = dR = -\sum N_1 \ . \tag{5-3}$$

Substituting for N_i

$$\frac{1}{K_1 P_2} \frac{dQ}{dA} = -\Sigma(P_r y_i - x_i)\alpha_{i,1} \ . \tag{5-4}$$

Component balance for component i across the feed side of the membrane reactor provides

$$Q y_i = (Q+dQ)(y_i+dy_i) + N_i \ . \tag{5-5}$$

Substituting for dQ and N_i and ignoring the second order terms

$$\frac{1}{K_1 P_2} \frac{dy_i}{dA} = \frac{y_i}{Q}\left[\sum (P_r y_i - x_i)\alpha_{i,1}\right] - (P_r y_i - x_i)\frac{\alpha_{i,1}}{Q} \ . \tag{5-6}$$

A similar component balance on the permeate side provides

$$\frac{1}{K_1 P_2} \frac{dx_i}{dA} = \frac{x_i}{R}\left[\sum (P_r y_i - x_i)\alpha_{i,1}\right] - (P_r y_i - x_i)\frac{\alpha_{i,1}}{R} \ . \tag{5-7}$$

For a cocurrent flow scheme, the equations describing dQ and dy_i remain the same, and in equations describing dR and dx_i, signs are reversed on the right side of the above equations, i.e.

$$\frac{1}{K_1 P_2} \frac{dR}{dA} = \Sigma(P_r y_i - x_i)\alpha_{i,1} \tag{5-8}$$

and

$$\frac{1}{K_1 P_2}\frac{dx_i}{dA} = -\frac{x_i}{R}\left[\sum (P_r y_i - x_i)\alpha_{i,1}\right] + (P_r y_i - x_i)\frac{\alpha_{i,1}}{R} \quad . \tag{5-9}$$

The permeability ratios $\alpha_{i,1}$ reflect the permeation mechanism for the gas species. For permeation dominated by Knudsen diffusion the $\alpha_{i,1}$ equals the inverse ratio of the square root of respective molecular weights:

$$\alpha_{i,1} = \sqrt{\frac{M_1}{M_i}} \quad . \tag{5-10}$$

The permeation of gases across the membrane changes the feed side gas composition as given by dy_i. Its effect on the WGS reaction is taken into account in this model by assuming continuous chemical reaction equilibrium on the feed side. Thus

$$\frac{Y_{H_2}\, Y_{CO_2}}{Y_{CO}\, Y_{H_2O}} = K_{eq} \, . \tag{5-11}$$

The model assumes isothermal reactor conditions; thus, the equilibrium constant is assumed to be constant throughout the reactor length.

The initial conditions are provided by the initial feed gas composition as supplied to the membrane reactor. A computer program MEM.BAS was written in BASIC computer language to solve the above equations for both cocurrent and countercurrent modes for simulation of a membrane reactor. For a given feed composition, pressure ratio, P_r, and relative permeabilities $\alpha_{i,1}$, the program calculates the compositions of the exit raffinate and permeate streams for a specified membrane reactor stage cutoff (a stage cutoff is defined as the ratio of permeate to feed flow rates). For a cocurrent mode, the numerical solution progresses from the feed side of the membrane reactor in a straightforward manner. Change in the residual and permeate mol fractions is computed for each small incremental change in total flow, dQ. After each dQ incremental computation, the feed side composition is updated to reflect a new chemical reaction equilibrium. The calculations continue until the desired permeate flow is reached.

For a countercurrent flow mode a trial-and-error procedure is necessary. A guess composition of the exit raffinate concentration needs to be provided to start the calculations. The calculations proceed from the raffinate exit end in a reverse order to the feed side. The computed feed composition is then compared with the specified feed composition to provide the error. A Newton-Raphson iteration procedure is used to update the guess concentration values. A first guess of the concentration values may be provided by running the program in a cocurrent mode with the specified conditions. The exit raffinate composition computed for the cocurrent mode can provide a good guess value for the trial-and-error procedure.

5.1 Model Simulation Result

A number of simulations were carried out with the computer model to determine the increase in CO conversion and the concentration of hydrogen in the product stream. The motivation for this project comes from its possible application in hydrogen production in coal liquefaction plants. For this application, a product hydrogen stream purity of 90 percent may be considered acceptable. Thus, simulations were conducted to identify scenarios under which the 90 percent hydrogen concentration level may be achievable. A typical MTCI char gasifier exit composition was used as feed composition for most of these simulations. The composition consisted of 48.6 percent H_2, 21.0 percent CO_2, 17.3 percent CO, and 13.1 percent N_2 on a dry basis. Three different steam-to-CO mol ratios of 2:1, 3:1, and 4:1 were used in these simulations. In all simulations the reactor temperature was assumed to be 425 °C with a corresponding WGS reaction equilibrium constant of 10.0.

For each of the steam-to-CO ratios used, simulations were conducted for different pressure ratios and stage cutoff values to obtain the CO conversion in the reactor as well as the concentration of hydrogen in the product permeate stream on a dry basis. Knudsen diffusion was assumed to be the dominant permeation mechanism to assign various gas permeability ratios. Thus, the following permeability ratios were used:

$$\alpha_{CO,H_2} = K_{CO} / K_{H_2} = 0.267$$
$$\alpha_{N_2,H_2} = K_{N_2} / K_{H_2} = 0.267$$
$$\alpha_{CO_2,H_2} = K_{CO_2} / K_{H_2} = 0.213$$
$$\alpha_{H_2O,H_2} = K_{H_2O} / K_{H_2} = 0.333 .$$

Figures 5-2, 5-3, and 5-4 indicate the predicted conversion of CO in a single-stage membrane reactor as a function of stage cut and pressure ratio. The percent CO conversion increases with both the pressure ratio and the stage cut. These simulations were conducted with cocurrent feed and permeate flows. The CO conversion at zero stage cut corresponds to that achieved with no membrane separation. Thus, comparison of an indicated CO conversion with that at zero stage cut directly indicates the effect of membrane separation on increase in CO conversion. As seen from these figures, the CO conversion increases only marginally for the low-pressure ratio of 2, and a high-pressure ratio of 10 to 20 is needed to increase the CO conversion significantly. At pressure ratios greater than 20, the incremental increase in CO conversion is relatively small. With a H_2O:CO mol ratio of 3:1, about 85 percent conversion of CO is predicted with a pressure ratio of 20 at a stage cut of 0.7, compared to 70 percent CO conversion without any membrane separation.

Figure 5-5 shows the model-predicted hydrogen concentration in the product permeate stream as a function of stage cut and pressure ratio for a steam-to-CO mol ratio of 3:1. The product hydrogen concentration predominantly depends on the permeability ratios used for different gases, thus the hydrogen concentrations were similar for other steam-to-CO mol ratio simulations. This figure indicates that at high-pressure ratios a single-stage membrane reactor will provide about

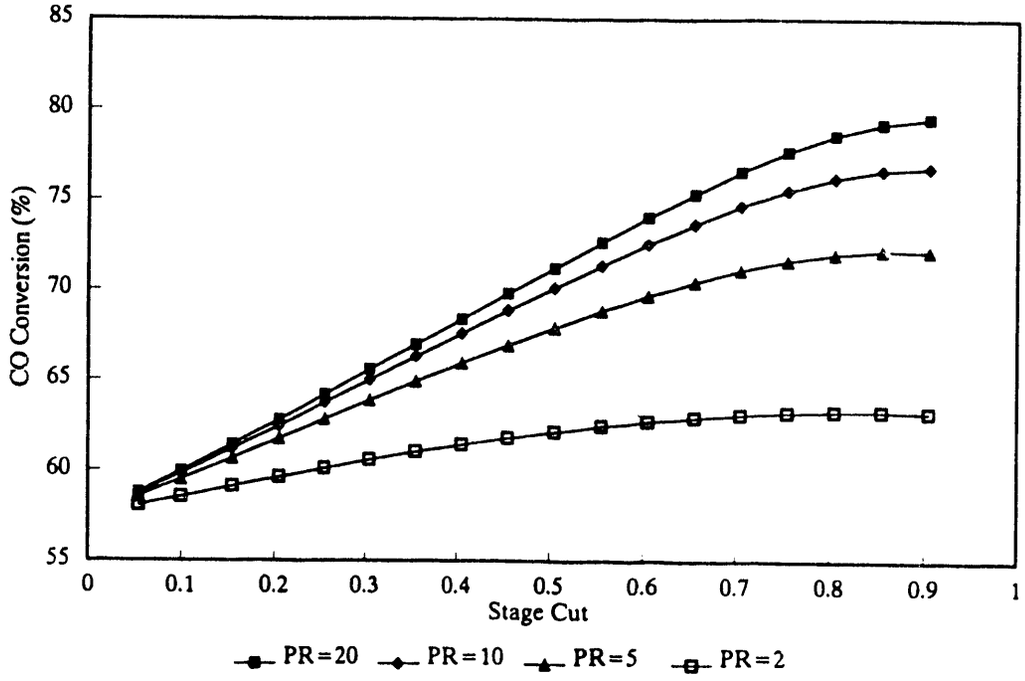

Figure 5-2. Effect of stage cut and pressure ratio on CO conversion, MTCI gasifier gas composition, H_2O:CO = 2:1.

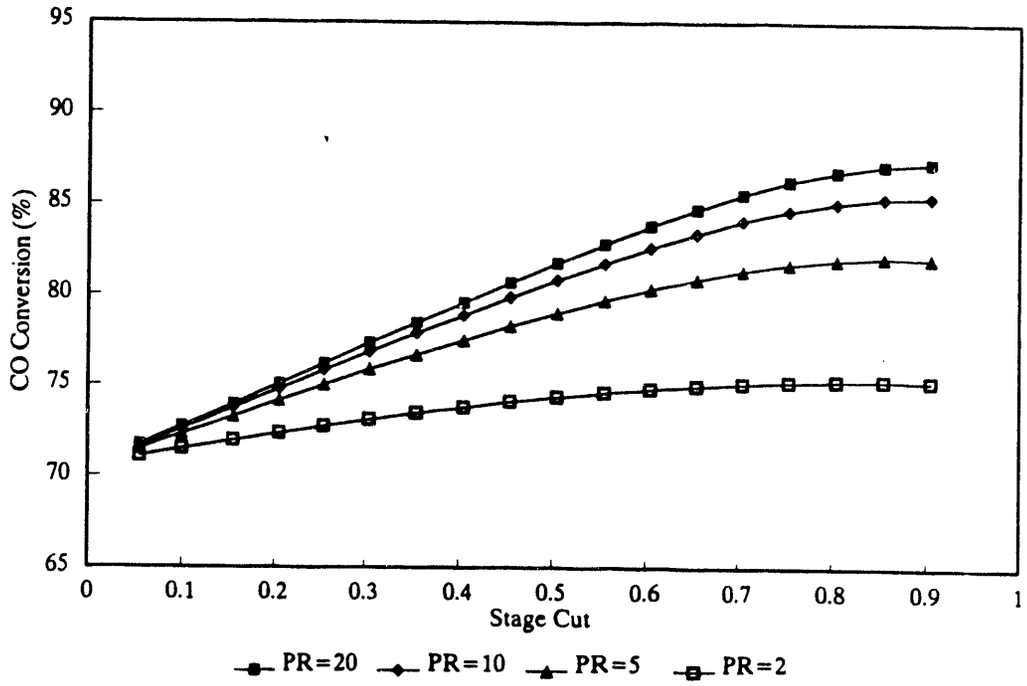

Figure 5-3. Effect of stage cut and pressure ratio on CO conversion, MTCI gasifier gas composition, H_2O:CO = 3:1.

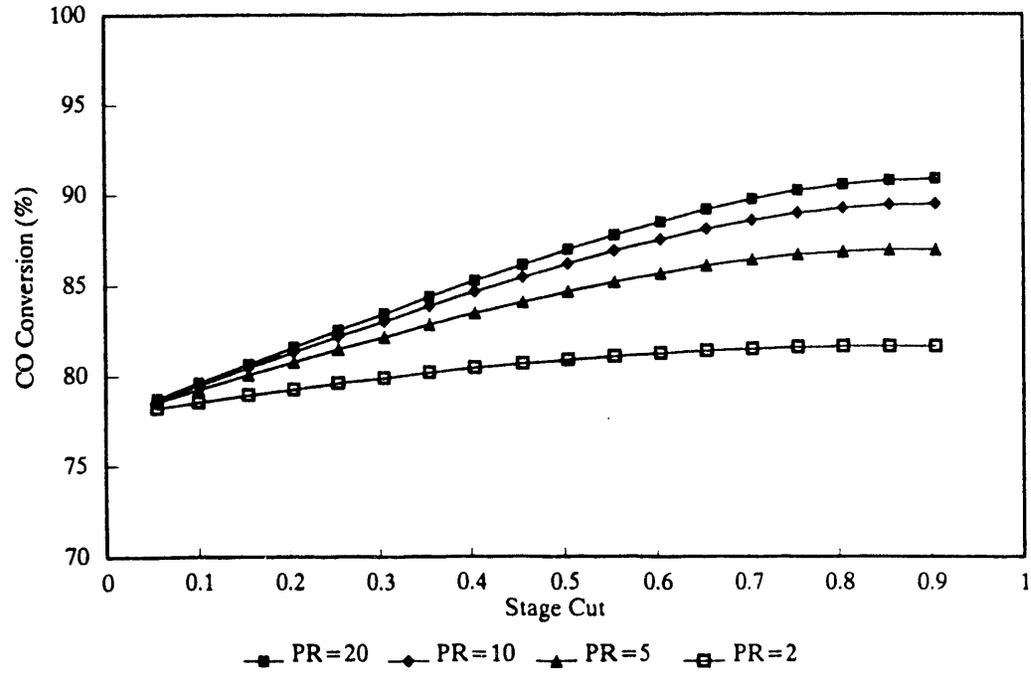

Figure 5-4. Effect of stage cut and pressure ratio on CO conversion, MTCI gasifier gas composition, H_2O:CO = 4:1.

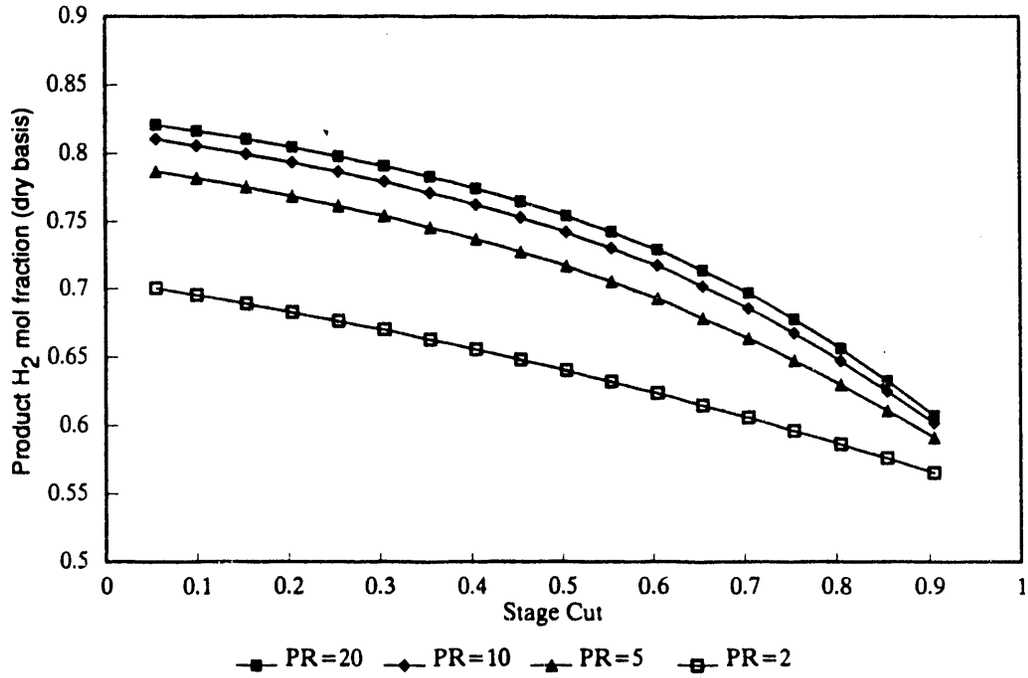

Figure 5-5. Effect of stage cut and pressure ratio on product H_2 concentration, MTCI gasifier gas composition, H_2O:CO = 3:1.

70 percent hydrogen concentration (dry basis) for a stage cut of 0.7. Such a high stage cut is needed for increasing overall hydrogen recovery in the product stream. As seen from this figure, higher hydrogen concentrations in the permeate stream are possible using a smaller stage cut value at the expense of reduced hydrogen recovery, e.g., for a feed of 1 mol, a 0.5 stage cut at a P_r of 20 will provide a 76 percent hydrogen stream with a hydrogen recovery of 0.38 mol, whereas a 0.7 stage cut at the same pressure ratio will provide a 70 percent hydrogen stream with a hydrogen recovery of 0.49 mol. This simulation result also indicates that more than one stage will be needed even with high-pressure ratio and ideal Knudsen separation to achieve a 90 percent hydrogen concentration with a reasonable hydrogen recovery.

Figures 5-6 and 5-7 show simulation results obtained with countercurrent feed and permeate flows. The predicted values with the countercurrent flow scheme are shown as open symbols; the lines with closed symbols indicate results of cocurrent flows under otherwise identical conditions. Figure 5-6 shows the predicted CO conversions with a H_2O:CO mol ratio of 3:1. As seen from this figure, a countercurrent flow scheme increases the CO conversion as compared to cocurrent flow. The difference is especially significant for smaller pressure ratios of 2 and 5, as expected. At a high-pressure ratio of 20, the difference in the two flow modes is small. Figure 5-7 compares the product hydrogen concentrations for the two flow modes. Again, the difference is significant for low-pressure ratios of 2 and 5 but is minimal for a high-pressure ratio of 20. As mentioned earlier, countercurrent simulations require a trial and error procedure, where the first trial may be provided by the cocurrent simulation results.

Because the gas separation factors observed with the carbon membranes so far tested were significantly less than the Knudsen diffusion separation factors, simulations were carried out with smaller values for the permeability ratios. The best observed H_2/CO_2 separation factor or the permeability ratio under high-pressure WGS reaction conditions is approximately 2.0 as seen in Table 4-4. Therefore, simulations were carried out using the following lower values for different permeability ratios based on the above observed value:

$$\alpha_{CO_2,H_2} = K_{CO_2} / K_{H_2} = 0.5$$
$$\alpha_{CO,H_2} = K_{CO} / K_{H_2} = 0.627$$
$$\alpha_{N_2,H_2} = K_{N_2} / K_{H_2} = 0.627$$
$$\alpha_{H_2O,H_2} = K_{H_2O} / K_{H_2} = 0.782 \quad .$$

Figure 5-8 shows the predicted CO conversion as a function of pressure ratio and stage cut for a steam-to-CO mol ratio of 3:1. As seen from this figure, the CO conversion was found to increase only marginally even at a high-pressure ratio of 20. The predicted CO conversion at a 0.7 stage cut was only about 72 percent as compared to 85 percent predicted with ideal Knudsen diffusion separation (Figure 5-3). At a low-pressure ratio of 2, the conversion was actually predicted to decrease with membrane separation. Such apparently anomalous behavior results from the high equilibrium constant of 10 used in the simulations, which requires a certain minimum hydrogen-to-CO permeation ratio in order to shift the equilibrium significantly enough to increase CO conversion. At the low-pressure ratio of 2, the permeation of CO through

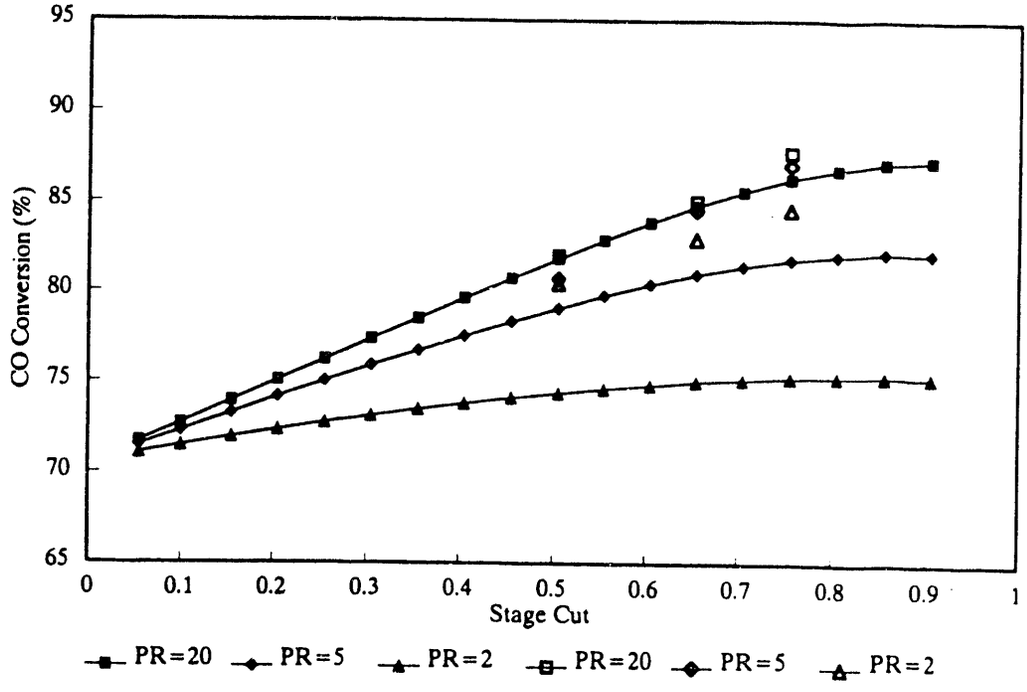

Figure 5-6. Effect of flow scheme on CO conversion, MTCI gasifier gas composition, H_2O:CO = 3:1.

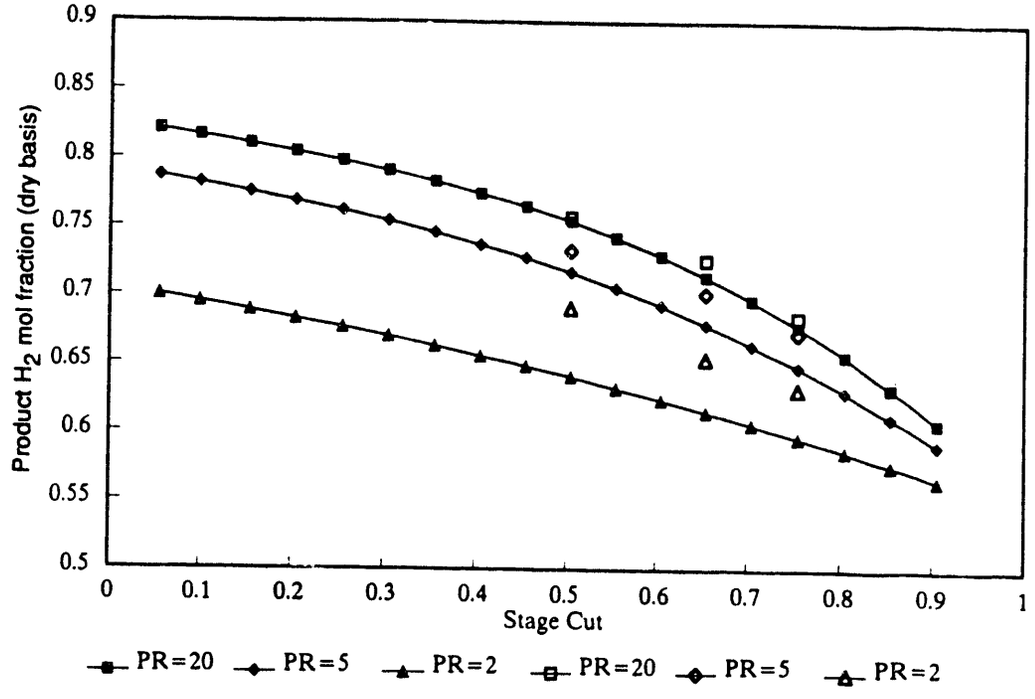

Figure 5-7. Effect of flow scheme on product H_2 concentration, MTCI gasifier gas composition, H_2O:CO = 3:1.

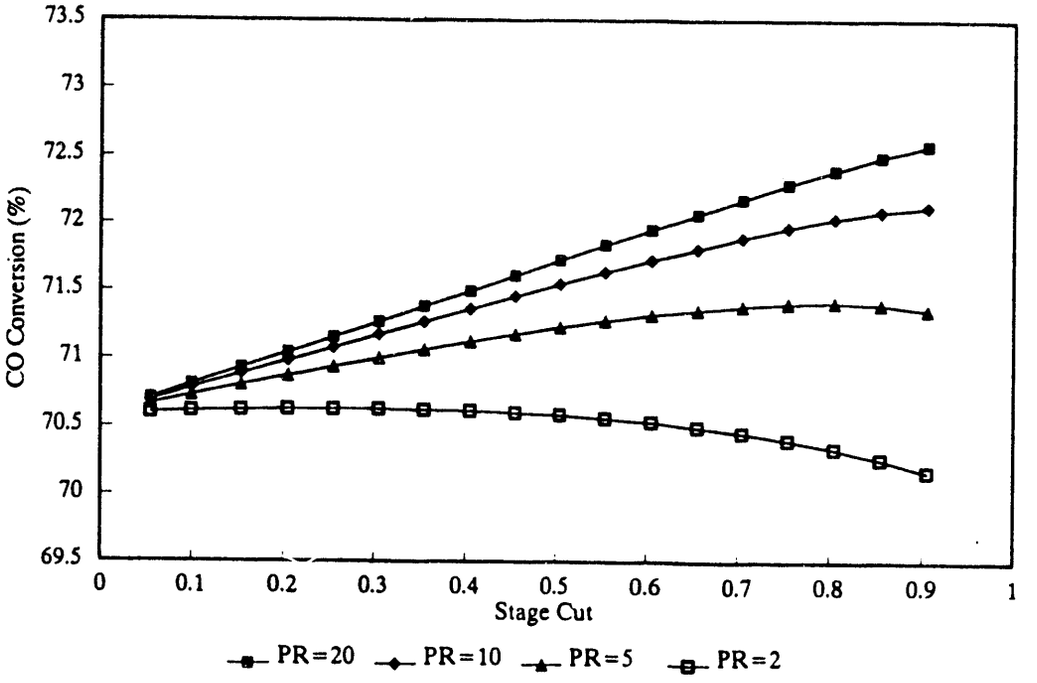

Figure 5-8. Effect of stage cut and pressure ratio on CO conversion, low gas separation factors, MTCI gasifier gas composition, H_2O:CO = 3:1.

the membrane was significant enough and thus it did not increase CO concentration on the feed side significantly to shift the equilibrium in the desired direction. Figure 5-9 shows the permeate hydrogen concentration as a function of pressure ratio and stage cut. Because the predicted increase in CO conversion was small even for a high-pressure ratio, the permeate hydrogen concentration values reflect a simple passive membrane separation with the low specified separation factors. At a stage cut of 0.7, the permeate hydrogen concentration was predicted to be only 62 percent. Thus, a large number of stages will be required (with a consequently low hydrogen recovery) to achieve the desired hydrogen concentration of 90 percent.

Additional model simulations were carried out to determine the effect of two and three stages on the product hydrogen concentration. During simulations it became apparent that only the first stage could be considered as a membrane reactor, as the product hydrogen-enriched stream, if subjected to further WGS reaction at the same temperature as in the first stage, would follow a reverse reaction. Thus, in these simulations, second and third stages were assumed to be that of passive membrane separations. A product stream with 0.75 stage cut of the first stage was used as a feed for the second stage, and the product stream with 0.75 stage cut of the second stage was used as the feed stream for the third stage. Figure 5-10 provides the predicted hydrogen product stream concentrations as a function of the number of stages obtained with Knudsen diffusion separations. This figure indicates that the two-stage process with a pressure ratio of 20 in each stage can provide a hydrogen concentration in the range of 85 percent, and

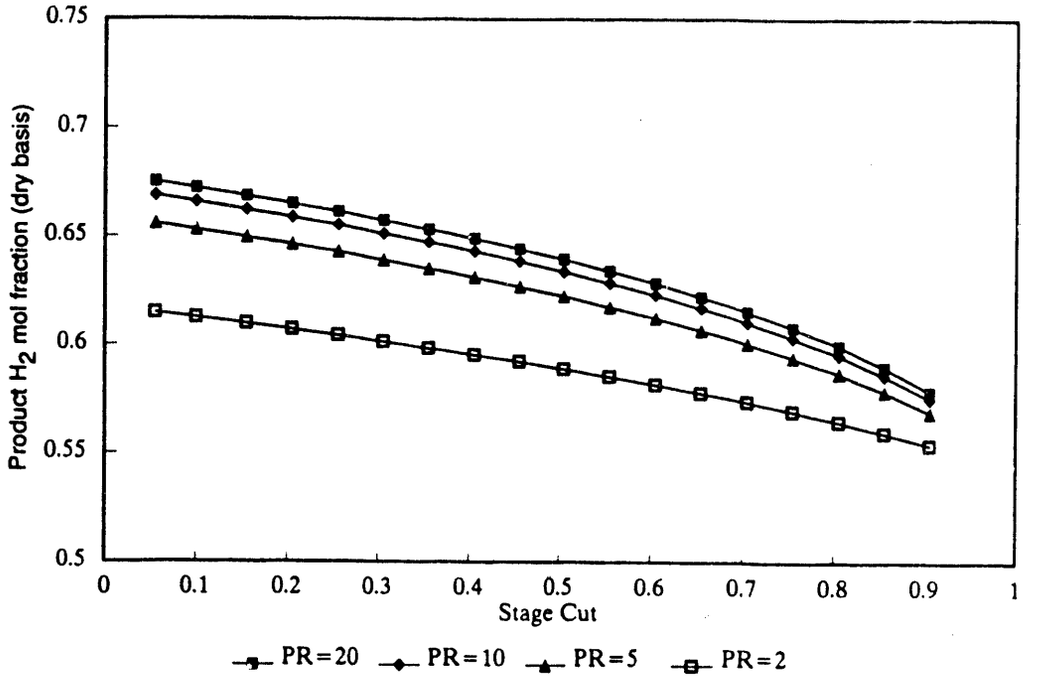

Figure 5-9. Effect of stage cut and pressure ratio on product H_2 concentration, low gas separation factors, MTCI gasifier gas composition, H_2O:CO = 3:1.

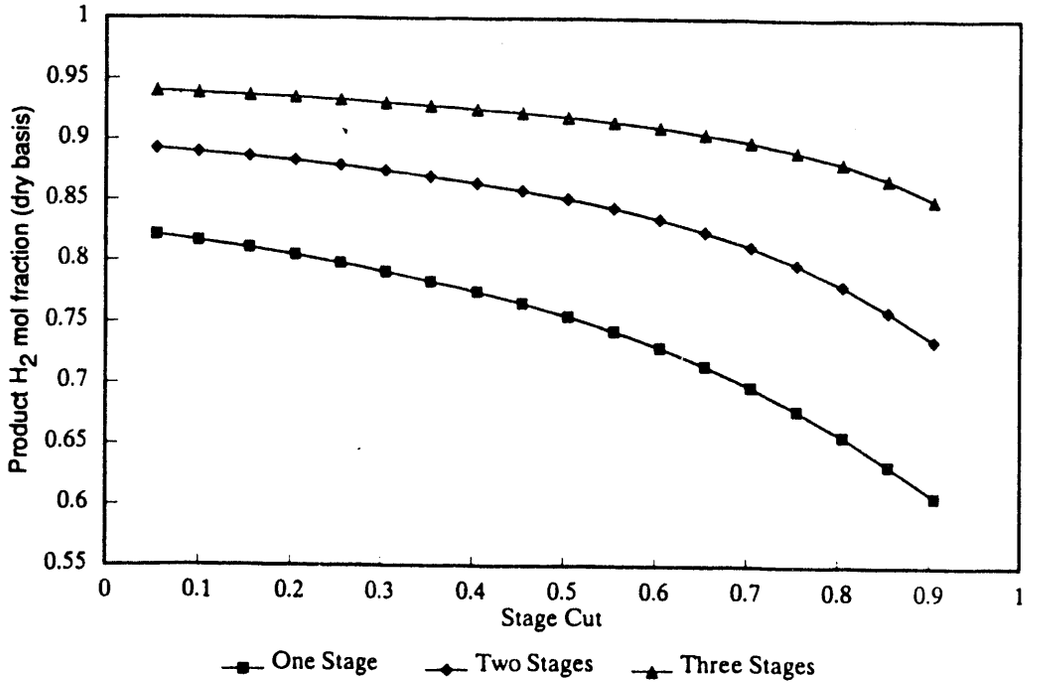

Figure 5-10. Product H_2 concentration with number of stages, MTCI gasifier gas composition, H_2O:CO = 3:1, Knudsen diffusion separation.

three stages are needed to increase the hydrogen purity above the desired 90 percent level. With a high-pressure ratio of 20, each additional stage would require a recompression of the product stream from a previous stage.

Figure 5-11 indicates simulation results obtained with low permeability ratios as experimentally observed with the carbon membranes. The results indicate that the hydrogen concentration in the permeate stream could be enriched only to 75 percent using three stages. More than five stages would thus be required to increase the hydrogen concentration in the product stream above 90 percent with a consequent reduction in hydrogen recovery.

Figures 5-12 through 5-14 indicate results obtained with a typical Texaco gasifier gas composition consisting of 36 percent H_2, 47 percent CO, and 17 percent CO_2. Two steam-to-CO ratios of 1:1 and 2:1 were used in these simulations. The results show trends similar to those seen in simulations with MTCI gasifier gas composition.

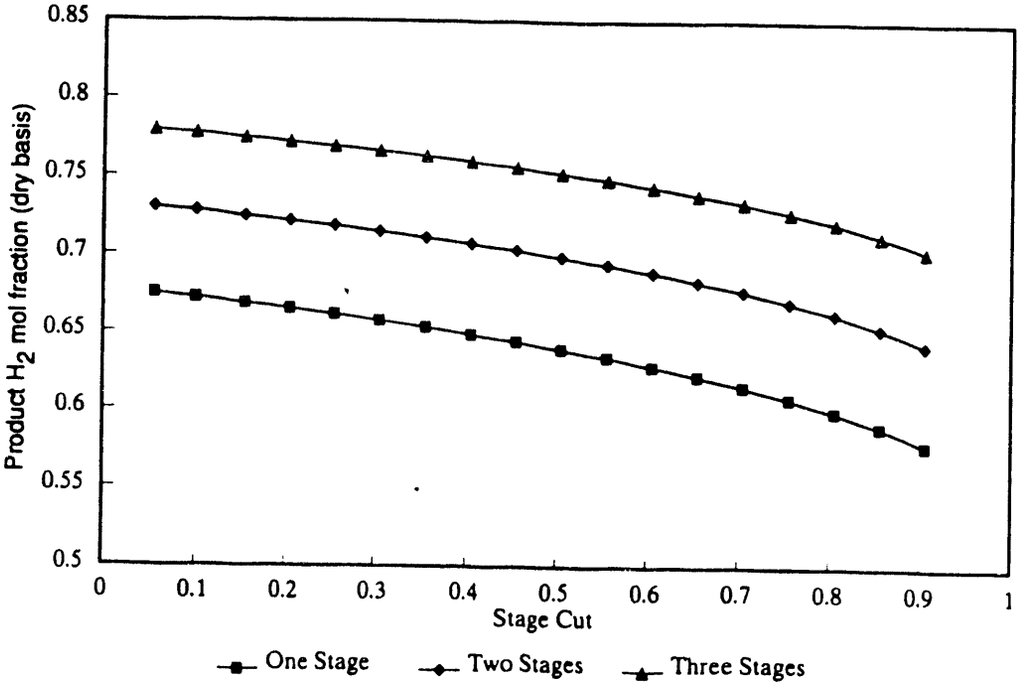

Figure 5-11. Product H_2 concentration with number of stages, MTCI gasifier gas composition, H_2O:CO = 3:1, low gas separation factors.

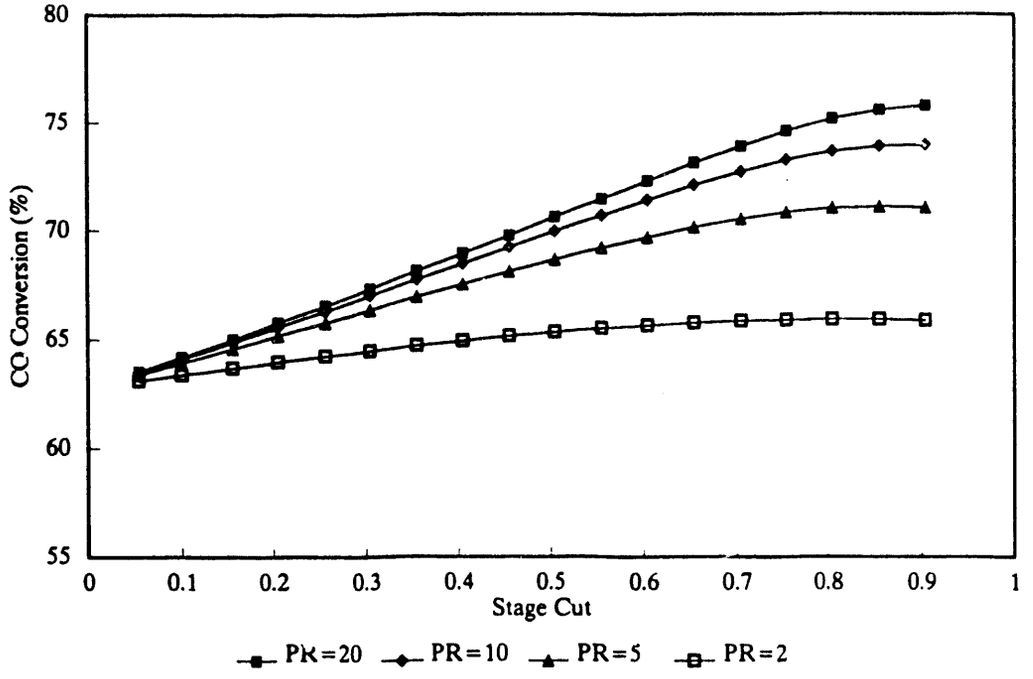

Figure 5-12. Effect of stage cut and pressure ratio on CO conversion, Texaco gasifier gas composition, H_2O:CO = 1:1.

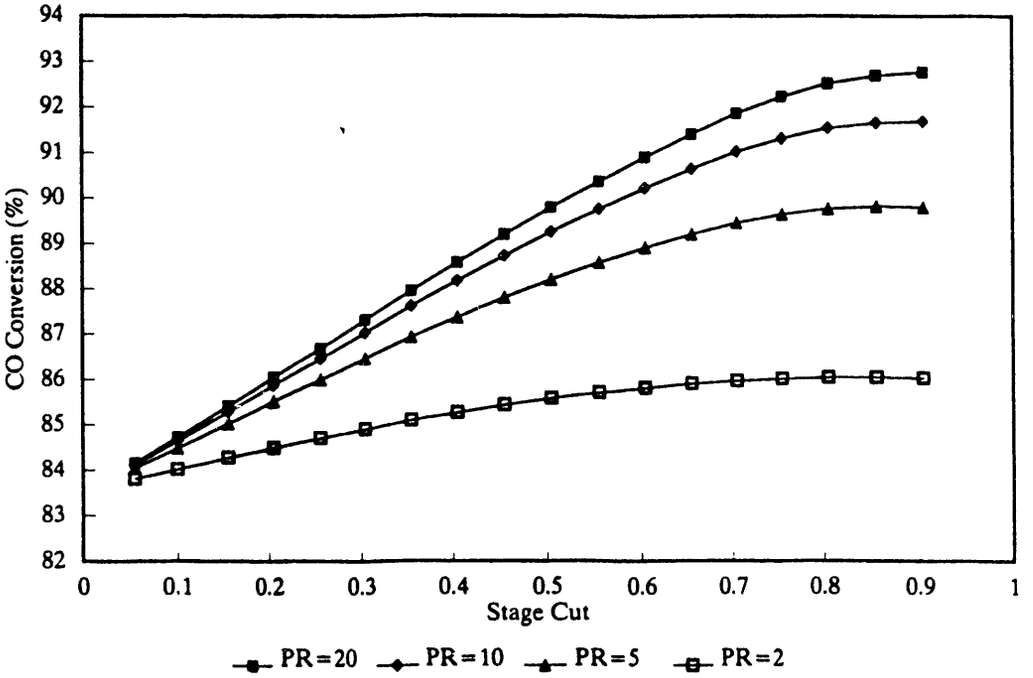

Figure 5-13. Effect of stage cut and pressure ratio on CO conversion, Texaco gasifier gas composition, H_2O:CO = 2:1.

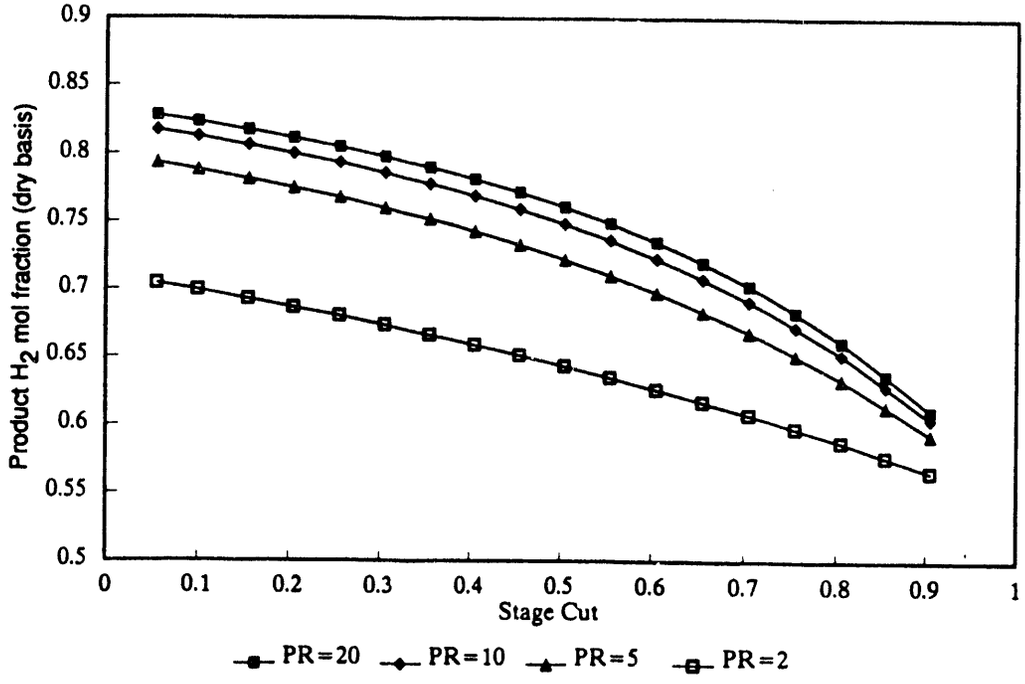

Figure 5-14. Effect of stage cut and pressure ratio on product H_2 concentration, Texaco gasifier gas composition, H_2O:CO = 2:1.

SECTION 6

CONCLUSIONS

Commercially available carbon composite microfiltration membranes were modified by depositing a layer of organic polymeric precursor on the microfiltration layer followed by controlled pyrolysis. Polymer precursor materials investigated in this project include PAN, PFA, phenol-formaldehyde resin, cellulose, FAP resin, and polyxylene. Precursor deposition techniques based on polymer solution coating, plasma polymerizations, and gas-phase pyrolysis decreased the gas permeation rates significantly; however, these techniques did not significantly improve gas separation ability.

The in situ polymerization technique was found to be much more promising, and pure component permeation tests with membrane samples prepared with this technique indicated predominantly diffusive flow. The hydrogen permeabilities of these membranes ranged from 1×10^{-5} to 5×10^{-5} std $cm^3/(s\cdot cm^2\cdot mm\ Hg)$ as compared to 6×10^{-3} std $cm^3/(s\cdot cm^2\cdot mm\ Hg)$ for an unmodified carbon microfiltration tube. The gas separation factors for these membranes at HTHP conditions were greater than those for an unmodified membrane; however, they were lower than theoretical maximum values for Knudsen diffusion separation. These factors also depended strongly on gas temperature and transmembrane pressure drop, indicating significant contribution of viscous flow especially at high-pressure conditions.

WGS reaction with simultaneous separation of hydrogen using the modified membranes indicated moderately increasing CO conversions with increasing hydrogen permeation. The stage cuts in these experiments were, however, small, on the order of 0.1 or less.

A simple process model was developed to simulate simultaneous WGS reaction and hydrogen separation based on continuous chemical reaction equilibrium and user-provided gas separation factors. With Knudsen diffusion separation, high-pressure ratios of 10 to 20 were found to be necessary to increase CO conversion and product hydrogen concentrations. A multistage process was found to be necessary to increase the hydrogen product concentration: a two-stage process providing 80 to 85 percent hydrogen and a three-stage process providing >90 percent hydrogen.

Model simulation with the gas separation factors observed in this project indicated a very small increase in CO conversion even with high-pressure ratio and stage cut. Also, simulations indicated that a large number of stages will be required to increase the hydrogen concentration to more than 80 percent. Thus, further improvement in the gas separation ability of the modified carbon membranes is necessary to make the concept of a catalytic carbon membrane reactor technically feasible.

Future work in this area may be directed toward making the carbon membrane gas separation layer defect-free so as to minimize the viscous contribution seen at high-pressure conditions. The

carbon membranes need to be fabricated in a module for testing in an actual coal gas environment. WGS reaction experiments need to be conducted under high stage cut conditions using longer membranes, to verify model predictions experimentally. Alternative approaches to Knudsen diffusion separation, based on molecular sieve-type carbon membranes, may be investigated to increase the hydrogen separation factors beyond the Knudsen diffusion limits.

SECTION 7

REFERENCES

Abotsi, G.M.K., 1987, Ph.D. Thesis, The Pennsylvania State University, University Park, Pennsylvania.

Abotsi, G.M.K., and A.W. Scaroni, 1989, "A Review of Carbon-Supported Hydrodesulfurization Catalysts," *Fuel Processing Technology,* 22:107-133.

Aldridge, C.L., and T. Kalina, 1971, German Patents 1,928,389; 1,959,012; 2,054,869; 2,054,946 (May 6, 1970 to May 19, 1971), Esso Research and Engineering Company.

Barrer, R.M., 1965, AIChE Symposium Series, 1:112.

Bartis, J.T., and L.S. Marks, 1984, Final Report, U.S. DOE Contract No. DE-AP21-84MC20159.

Berispek, V., 1975, "Studies of an Alkali Impregnated Cobalt-Molybdate Catalyst for the Water-Gas Shift and the Methanation Reactions," M.S. Thesis, VPI and SV, March.

Bohlbro, H., and M.H. Jorgensen, 1970, *Chem. Eng. World,* 5:46.

Brinen, J.S., and W.D. Armstrong, 1958, *J. Catal.,* 54:57.

Butterworth, S.L., and A.W. Scaroni, 1985, *Applied Catalyst,* 16:375-388.

Chadwick, D., et al., 1983, *Preparation of Catalysts,* 3:323.

Daly, F.F., and J.S. Brinen, 1987, *Applied Catalysis,* 30:991-997.

Derbyshire, F.J., V.H.J. de Beer, G.M.K. Abotsi, A.W. Scaroni, J.M. Solar, and D.J. Skrovanek, 1986, "The Influence of Surface Functionality on the Activity of Carbon-Supported Catalyst," *Applied Catalysis,* 27:117-131.

Fleming, H.L., 1988, "Carbon Composite: A New Family of Inorganic Membranes," Sixth Ann. Membr. Plan. Conf., Cambridge, MA, November.

Furimsky, E., 1980, *Catal. Rev. Sci. Eng.,* 22(3):371-400.

Grange, P., 1980, "Catalytic Hydrodesulfurization," *Catal. Rev. Sci. Eng.,* 22(3):371-400.

Harris, L., 1964, German Patent 1,162,502 (February 6), Peter Spence and Sons, Ltd.

Havredaki, V., and J.H. Petropoulos, 1983, *J. Membrane Sci.,* 12:303.

Hippo et al., 1979, *Fuel,* 58:338.

Hsieh, H.P., 1988, "Inorganic Membranes," AIChE Symposium Series 261, K.K. Sirkar and D.R. Lloyd, eds., 1:84.

Hucke, E.E., 1975, U.S. Patent 3,859,421, January 7.

Kameyama, T., M. Dokiya, K. Fulcuda, and Y. Kotera, 1979, *Sep. Sci. and Technology,* 14:953.

Kettman, V., P. Balgavy, and L. Sokol, 1988, *J. Catal.,* 112:93-106.

Kolboe, S., and C.H. Amberg, 1966, *Can. J. Chem.,* 44:2623.

Koresh, J.E., and A. Sofer, 1983, "Molecular Sieve Carbon Permselective Membrane. Part I: Presentation of a New Device for Gas Mixture Separation," *Sep. Sci. and Technology,* 18(8):723-734.

Kotera, Y., K. Ogawa, M. Oba, K. Shimomyra, M. Yonemura, A. Veno, and N. Rodo, 1976, *Preparation of Catalysts,* 1:372.

Lee, K.H., and S.J. Khang, 1986, *Chem. Eng. Commun.,* 44:121.

Levinson, G.S., et al., 1974, German Patent 2,416,351, Shell Internationalle Research, Maatschappij B.V., October 24.

Merango et al., 1983, *Preparation of Catalysts,* 3:359.

Markina, M.I., and G.K. Boreskov, 1961, In F.P. Vanowkii, and B.G. Lyudkovsbaya, eds., *Kinet. Katl.,* 2:867.

Morita, Y., and K. Ysuchimoto, 1967, *Nnryo Kyokai-Shi,* 46:802.

Neely, J.W., 1981, *Carbon,* Pergamon Press, 19:27-36.

Neely, J.W., and E.G. Isacoff, 1982, "Carbonaceaous Adsorbents for the Treatment of Ground and Surface Waters," Marcel Dekker, Inc., New York and Basel.

Newling, W.B.S., and J. Rich, 1966, *Gas (Rome),* 16:233.

Newsome, D.S., 1980, *Catal. Rev. Sci. Eng.,* 21(2):275-318.

Oades, R.D., S.R. Morris, and R.B. Moyes, 1989, "Carbon Supported Molybdenum and Molybdenum-Potassium Catalysts for the Hydrogenation of Carbon Monoxide," In

Proceedings of the Carbons and Catalysis Conference, September 11-13, Loughborough University of Technology, England, to appear in *Catalysis Today.*

Ontsuka, T., 1977, *Catal. Rev. Sci. Eng.*, 16(2):291-325.

Overstreet, A.D., 1974, "A Screening Study of a New Water-Gas Shift Catalyst," M.S. Thesis, VPI and SU, July.

Owens, P.J., and C.H. Amberg, 1961, "Thiophene Desulfurization by a Microreactor Technique," *Adv. in Chem. Series, Am. Chem. Soc.,* 33:182.

Prins, R., V.H.J. de Beer, and G.A. Somorjai, 1989, *Catal. Rev. Sci. Eng.,* 31(1&2):1-41.

Ramselaar, W.L.T.M., R.H. Hadders, E. Gerkema, V.M.J. DeBeer, E.M. Van Oers, and A.M. Van DerKraan, 1989, *Applied Catalysis,* 51:263-283.

Reitz, O., and E. Lorenz, 1963, British Patent 940,960, Badische Anilin- and Soda-Fabrik A.-G., November 6.

Riley, K.L., and C.L. Aldridge, 1977, U.S. Patent 4,054,644, Exxon Research and Engineering Company, October 18.

Schmitt, J.L., Jr., and P.L. Walker, Jr., 1971, *Carbon,* 9:791.

Schmitt, J.L., Jr., and P.L. Walker, Jr., 1972, *Carbon,* 10:87.

Schmitt, J.L., Jr., P.L. Walker, Jr., and G.A. Castellion, 1976, U.S. Patent 3,987,000, August 31.

Segura, M.A., et al., 1976, U.S. Patent 3,974,094, Exxon Research and Engineering Company, August 10.

Scaroni, A.W., 1981, Ph.D. Thesis, Pennsylvania State University.

Scaroni, A.W., F.J. Derbyshire, M.K. Godfried, and J.M. Solar, 1987, U.S. Department of Energy Report, DOE/PC/G0050-12, June.

Scaroni, A.W., R.G. Jenkins, J.R. Utrilla, and P.L. Walker, Jr., 1984, *Fuel Processing Technology,* 9:103.

Singh, C.P.P., and D.N. Saraf, 1977, *Industrial and Engineering Chemistry Process Design and Development,* 16(3).

Sofer, A., J.E. Koresh, and S. Saggy, U.S. Patent No. 4685940, 1987.

Sherwood, P.W., 1961, *Petroleum (London),* 338.

Stevens, G.C., and T. Edmonds, 1979, Preparation of Catalysts II, Elsevier, pp. 508-517.

Topsoe, H., B.S. Clausen, N. Burriesci, R. Candia, and S. Morup, 1979, Preparation of Catalysts II, Elsevier, pp. 479-487.

Tsuchimota K., Y. Morita, and K. Yamamoto, 1968, *Kogyo Kajaku Zasshi,* 71:1488.

Urban, P., and D.J. Albert, 1973, U.S. Patent 3,725,303, April 3.

Venter et al., 1987, *J. Catalyst,* 103:450-465.

Walker, P.L., 1962, *American Scientist,* June:259-292.

Walker, P.L., 1978, Proc. 5th London Int. Carbon Graphite Conf., *Soc. Chem. Ind.,* 1:427.

Walker, P.L., Jr., T.C. Lamond, and J.E. Metcalfe III, 1966, Second Industrial Carbon and Graphite Conference, S.C.I., London, pp. 7-14.

Walker, P.L., Jr., A. Oya, and O.P. Mahajan, 1977, Abstracts, Thirteenth Biennial Conrerence on Carbon, ACS, pp. 382-383.

Walker, P.L., A. Oya, and O.P. Mahajan, 1980, *Carbon,* Pergammon Press, 18:377-378.

Wustrow, W., O. Maedrich, and H. Macura, 1954, German Patent 1,086,287, Ruhrgas A.-G., Applied June 28.

APPENDIX A
Listing of the MEMBRANE.BAS Computer Program

```
10 REM
20 REM                    RTI Membrane Reactor Model
30 REM                    Developed by Dr. A. S. Damle
40 REM                         (919) 541-8029
50 REM
60 REM  A five component reaction/membrane separation system is considered
70 REM  to simulate simultaneous Water-Gas-Shift (WGS) reaction and membrane
80 REM  separation in a membrane reactor:
90 REM
100 REM         Component 1 - Hydrogen
110 REM         Component 2 - Carbon Monoxide
120 REM         Component 3 - Carbon Dioxide
130 REM         Component 4 - Nitrogen, and
140 REM         Component 5 - Water.
150 REM
160 REM  The gas separation factors of each component with respect to
170 REM  hydrogen and the feed gas concentrations are provided by the user.
180 REM  The user also needs to provide the membrane operating conditions of
190 REM  pressure ratio and stage cut fraction. Both the co-current and
200 REM  counter-current flow modes are allowed. The counter-current flow
210 REM  mode uses a trial and error procedure and the user needs to provide
220 REM  the first guess values of the exit raffinate stream component mole
230 REM  fractions. In case of a co-current mode simulation the calculations
240 REM  are straight-forward and the results are saved in a user designated
250 REM  file. A co-current mode simulation can often provide good guess
260 REM  values for a counter-current mode simulation.
270 REM  The program may be run in a passive non-reactive mode or an active
280 REM  reactive mode. In the latter case, a continuous reaction equilibrium
290 REM  is assumed on the feed side and the feed side concentrations after
300 REM  each time step are updated to reflect the chemical equilibrium. The
310 REM  equilibrium constant for the WGS reaction (EQ) is provided by the
320 REM  user and is related to the feed side concentrations by:
330 REM
340 REM                    Y(1)*Y(3)
350 REM            EQ =  ---------  .
360 REM                    Y(2)*Y(5)
370 REM
380 REM  ************************************************************************
390 REM
400 REM  Initialization of variables and
410 REM  Interactive User Input
420 REM
430 DIM  Y0(5),Y(5),X(5),PARAM(5),ALPHA(5),YE(5),XE(5),DY(5),DX(5)
```

```
440 N=5:CLS:PRINT"":PRINT"":PRINT"    RTI Membrane reactor Model":PRINT""
450 Y0(1)=.3199:Y0(2)=.1139:Y0(3)=.1382:Y0(4)=.0862:Y0(5)=.3417
460 ALPHA(1)=1!:ALPHA(2)=.267:ALPHA(3)=.213:ALPHA(4)=.267:ALPHA(5)=.333
470 EQ=10:IMODE=1:MMODE=1:PR=20:F=.5
480 FOR I=1 TO N
490 PRINT" Feed Concentration of Component";I;" (";Y0(I);")";:INPUT C$
500 IF C$ < > "" THEN Y0(I)=VAL(C$)
510 IF I=1 GOTO 540
520 PRINT" Relative Permeability w.r.t Component 1 ";"(";ALPHA(I);")";:INPUT C$
530 IF C$ < > "" THEN ALPHA(I)=VAL(C$)
540 NEXT I
550 PRINT" Pressure Ratio P1/P2 - (";PR;")";:INPUT C$
560 IF C$ < > "" THEN PR=VAL(C$)
570 PRINT" Stage Cutoff Fraction - (";F;")";:INPUT C$
580 IF C$ < > "" THEN F=VAL(C$)
590 PRINT" Membrane Mode - (";MMODE;")";" : 1 - Active with reaction"
600 INPUT"                    2 - Passive with no reaction - ";MMODE
610 IF MMODE < > 2 THEN MMODE = 1
620 IF MMODE=2 GOTO 650
630 PRINT" Equilibrium Constant - (";EQ;")";:INPUT C$
640 IF C$ < > "" THEN EQ=VAL(C$)
650 PRINT" Flow Mode - (";IMODE;") : 1 - Cocurrent"
660 INPUT"                  2 - Countercurrent - ";IMODE
670 IF IMODE < > 2 THEN IMODE = 1
680 IF IMODE=2 GOTO 750
690 PRINT"":INPUT" Enter a Filename to save results e.g. DUMMY.OUT - ";F$
700 IF F$ = "" THEN F$ = "DUMMY.OUT"
710 OPEN "O", 1, F$
720 REM
730 REM  Co-current mode simulation
740 REM
750 IF IMODE>1 GOTO 1400
760 Q=1!:DQ=-.005:R=0!:C0=Y0(2):Q1=.05
770 FOR I=1 TO N
780 Y(I) = Y0(I)
790 NEXT I
800 IF MMODE=2 GOTO 820
810 GOSUB 2400
820 SUM = 0!
830 FOR I=1 TO N
840 SUM = SUM + Y(I)*ALPHA(I)
850 NEXT I
860 FOR I=1 TO N
870 X(I) = Y(I)*ALPHA(I)/SUM
880 NEXT I
890 PRINT Q;Y(1);Y(2);Y(3);Y(4);Y(5)
```

```
900 PRINT R;X(1);X(2);X(3);X(4);X(5)
910 GOSUB 2520
920 FOR I = 1 TO N
930 Y(I) = (Y(I) + DQ*X(I))/(Q+DQ)
940 NEXT I
950 XOLD=X(1)
960 SUMPA = 0!
970 FOR I = 1 TO N
980 PARAM(I) = (PR * Y(I) - X(I)) * ALPHA(I)
990 SUMPA = SUMPA + PARAM(I)
1000 NEXT I
1010 FOR I = 1 TO N
1020 X(I) = PR*Y(I) / (1+SUMPA/ALPHA(I))
1030 IF X(I) < 0  THEN X(I)=.0001
1040 NEXT I
1050 CHANGE = ABS((XOLD-X(1))/XOLD)
1060 IF CHANGE < .01 GOTO 1080
1070 GOTO 950
1080 Q = Q + DQ : R = R - DQ
1090 PRINT Q;Y(1);Y(2);Y(3);Y(4);Y(5)
1100 PRINT R;X(1);X(2);X(3);X(4);X(5)
1110 GOSUB 2520
1120 IF MMODE=2 GOTO 1140
1130 GOSUB 2400
1140 SUMPA = 0!
1150 FOR I = 1 TO N
1160 PARAM(I) = (PR * Y(I) - X(I)) * ALPHA(I)
1170 SUMPA = SUMPA + PARAM(I)
1180 NEXT I
1190 P2KADA=DQ/SUMPA
1200 FOR I = 1 TO N
1210 DY(I) = (SUMPA * Y(I) - PARAM(I)) * P2KADA / Q
1220 Y(I) = Y(I) - DY(I)
1230 DX(I) = (PARAM(I) - SUMPA * X(I)) * P2KADA / R
1240 X(I) = X(I) - DX(I)
1250 NEXT I
1260 Q = Q + DQ : R = R - DQ
1270 IF R=>F GOTO 1300
1280 IF R < Q1 GOTO 1120
1290 Q1 = Q1 + .05
1300 PRINT Q;Y(1);Y(2);Y(3);Y(4);Y(5)
1310 PRINT R;X(1);X(2);X(3);X(4);X(5)
1320 GOSUB 2520
1330 IF R=>F GOTO 1350
1340 GOTO 1120
1350 CLOSE 1
```

```
1360 STOP
1370 REM
1380 REM  Counter-current mode simulation
1390 REM
1400 Q=1-F:DQ=.005:R=0:C0=Y0(2):Q1=Q+.05
1410 FOR I=1 TO N
1420 Y(I) = Y0(I)
1430 NEXT I
1440 IF MMODE=2 GOTO 1460
1450 GOSUB 2400
1460 FOR I=1 TO N
1470 YE(I) = Y(I)
1480 NEXT I
1490 FOR I = 1 TO N
1500 PRINT" Guess Value for Raffinate Conc. of Component ";I;" - ";
1510 INPUT YR(I)
1520 Y(I) = YR(I)
1530 NEXT I
1540 Y1=YR(1):ITER=1:E1=0!:E2=0!
1550 PRINT ITER
1560 SUM = 0!
1570 FOR I=1 TO N
1580 SUM = SUM + Y(I)*ALPHA(I)
1590 NEXT I
1600 FOR I=1 TO N
1610 X(I) = Y(I)*ALPHA(I)/SUM
1620 NEXT I
1630 PRINT Q;Y(1);Y(2);Y(3);Y(4);Y(5)
1640 PRINT R;X(1);X(2);X(3);X(4);X(5)
1650 FOR I = 1 TO N
1660 Y(I) = (Q*Y(I) + DQ*X(I))/(Q+DQ)
1670 NEXT I
1680 XOLD=X(1)
1690 SUMPA = 0!
1700 FOR I = 1 TO N
1710 PARAM(I) = (PR * Y(I) - X(I)) * ALPHA(I)
1720 SUMPA = SUMPA + PARAM(I)
1730 NEXT I
1740 FOR I = 1 TO N
1750 X(I) = PR*Y(I) / (1+SUMPA/ALPHA(I))
1760 IF X(I) < 0  THEN X(I)=.0001
1770 NEXT I
1780 CHANGE = ABS((XOLD-X(1))/XOLD)
1790 IF CHANGE < .01 GOTO 1810
1800 GOTO 1680
1810 Q = Q + DQ : R = R + DQ
```

```
1820 PRINT Q;Y(1);Y(2);Y(3);Y(4);Y(5)
1830 PRINT R;X(1);X(2);X(3);X(4);X(5)
1840 IF MMODE=2 GOTO 1860
1850 GOSUB 2400
1860 SUMPA = 0!
1870 FOR I = 1 TO N
1880 PARAM(I) = (PR * Y(I) - X(I)) * ALPHA(I)
1890 SUMPA = SUMPA + PARAM(I)
1900 NEXT I
1910 P2KADA=DQ/SUMPA
1920 FOR I = 1 TO N
1930 DY(I) = (PARAM(I) - SUMPA * Y(I)) * P2KADA / Q
1940 Y(I) = Y(I) + DY(I)
1950 DX(I) = (PARAM(I) - SUMPA * X(I)) * P2KADA / R
1960 X(I) = X(I) + DX(I)
1970 NEXT I
1980 Q = Q + DQ : R = R + DQ
1990 IF Q < Q1 GOTO 2030
2000 Q1 = Q1 + .05
2010 PRINT Q;Y(1);Y(2);Y(3);Y(4);Y(5)
2020 PRINT R;X(1);X(2);X(3);X(4);X(5)
2030 IF MMODE=2 GOTO 2050
2040 GOSUB 2400
2050 IF R < F GOTO 1860
2060 IF ITER=1 GOTO 2220
2070 SUME=0
2080 FOR I = 1 TO N
2090 SUME = SUME + (YE(I)-Y(I))*(YE(I)-Y(I))
2100 NEXT I
2110 E2 = SUME^.5
2120 IF ABS(E2) < .02 GOTO 2340
2130 YNEW = Y1 - E1 * (Y1 - Y2) / (E1 - E2)
2140 IF ABS(E1) > ABS(E2) THEN Y1=Y2
2150 IF ABS(E1) > ABS(E2) THEN E1=E2
2160 ITER=ITER+1:Y2=YNEW:Y(1)=Y2:Q=1-F:R=0: FACTOR=(1!-Y2)/(1!-YR(1)):
     YR(1) = Y2
2170 Q1 = Q + .05
2180 FOR I = 2 TO N
2190 YR(I) = FACTOR * YR(I) : Y(I) = YR(I)
2200 NEXT I
2210 GOTO 1550
2220 SUME=0
2230 FOR I = 1 TO N
2240 SUME = SUME + (YE(I)-Y(I))*(YE(I)-Y(I))
2250 NEXT I
2260 E1 = SUME^.5
```

```
2270 IF ABS(E1) < .02 GOTO 2340
2280 Y2=Y1*.99:Y(1)=Y2:Q=1-F:R=0:ITER=ITER+1:FACTOR=(1!-Y2)/(1!-Y1):
     YR(1)=Y2
2290 Q1 = Q + .05
2300 FOR I = 2 TO N
2310 YR(I) = FACTOR * YR(I) : Y(I) = YR(I)
2320 NEXT I
2330 GOTO 1550
2340 PRINT"":PRINT"  Solution Converged !!":PRINT""
2350 PRINT" Final Exit Concentrations - "
2360 PRINT" Raffinate side -- ";:PRINT YR(1);YR(2);YR(3);YR(4);YR(5)
2370 PRINT" Permeate Side -- ";:PRINT X(1);X(2);X(3);X(4);X(5)
2380 STOP
2390 '
2400 AA = EQ - 1!
2410 BB = - Y(1) - Y(3) - (Y(2) + Y(5)) * EQ
2420 CC = EQ * Y(2) * Y(5) - Y(1) * Y(3)
2430 ARG = BB*BB - 4 * AA * CC
2440 IF ARG > 0 GOTO 2470
2450 SQRT = 0
2460 GOTO 2480
2470 SQRT = (BB*BB - 4! * AA * CC) ^ .5
2480 FF = (- BB - SQRT) / 2! / AA
2490 Y(1) = Y(1) + FF : Y(3) = Y(3) + FF
2500 Y(2) = Y(2) - FF : Y(5) = Y(5) - FF
2510 RETURN
2520 CON = (1-(Q*Y(2)+R*X(2))/C0)*100
2530 H2DRYP = X(1)/(1!-X(5))
2540 H2DRYR = Y(1)/(1!-Y(5))
2550 PRINT "  Permeate Flow Moles =";R
2560 PRINT# 1,R,CON,H2DRYP,H2DRYR,X(1),X(2),X(3),X(4),X(5),Y(1),Y(2),
     Y(3),Y(4),Y(5)
2570 PRINT "  CO Conversion (%) =";CON
2580 PRINT "  H2 Mole Fraction in Permeate (Dry basis) =";H2DRYP
2590 PRINT "  H2 Mole Fraction in Residue (Dry basis) =";H2DRYR
2600 PRINT""
2610 RETURN
```

END

DATE
FILMED
8/11/92